
**Final Report**

# Adaptive Control of an Active Pneumatic Damper

**Presented to:**

**Dr. Nasim Daher**

**Presented by:**

**A. Kourani  A. Koleilat &, P. El Haddad**

**Adaptive Control**

**May 2016**

# Contents

# Adaptive Control of an Active Pneumatic Damper

## I. Introduction

The circulatory system can be comparable to a hydraulic system were the heart is represented by a pump, and the veins and arteries are represented by pipes. This comparison makes it easier to develop an adaptive control system to regulate pressure and flow inside veins and arteries in the face of unknown disturbances. The reason the heart is compared to a pump, is that when it contracts it pumps blood out at high pressure, and when it relaxes to be filled with blood it causes a drop in pressure of the blood in the veins and arteries, just like a pump does to water. This is known in biology as systole (at contraction) and diastole (at relaxation). To simplify the complex circulatory system for our analysis we will be using set up using a pump, two tanks, pipes, and pneumatic valves. The pump will feed water to a pipe that will fill the first tank inside which pressure will be measured and controlled by the flow of compressed air that is controlled by a pneumatic valve. The output water from the tank will be at constant desired flow rate and pressure. The controlled water flow in the pipes will then get redirected to the second tank were the same process is repeated before the water gets sucked back is to the pump. We will model our pipes as hydraulic resistances and impedance for simplicity. To introduce disturbances to our system we could reduce the power input to our pump, or even add clamps to our pipes to restrict water flow on different locations. The reason for using water instead of blood, other that convenience is that we cannot find a pump suited for blood on the market.

## II. Literature review

**Efficient anisotropic adaptive discretization of the cardiovascular system [6]:**
This paper demonstrate how computational efficiency can be increased in simulating a cardiovascular flow by using an anisotropic adaptive discretization method. They propose a new adaptive approach that controls the mesh adaptation procedure to obtain more accurate wall shear stress computation. Finite element formulation for the transient incompressible Navier–Stokes equation governing blood flow are presented, as well as detailed wall shear stress numerical computation. The accuracy of the solution depends on subdividing the domain into a finite number of elements called mesh. In the blood flow problem the solution exhibits strong anisotropic features that requires a lot of elements. The problem is solved by iterative adaptive procedure where the errors introduced due to spatial discretization are controlled within a specified tolerance. The anisotropic adaptive procedure makes the mesh resolution adequate in all directions. They analyse the strengths and weaknesses of tow classes of meshing strategies, anisotropic adaptivity and pre-defined boundary layer meshing. They then propose a new approach that combines the two strategies and demonstrated its efficiency.

**Multiple-Model Adaptive Predictive Control of Mean Arterial Pressure and Cardiac Output [7]:**

In this paper a multiple-model adaptive controller (MMAC) has been designed to regulate cardiac output and arterial pressure by adjusting the infusion rate of nitroprusside and dopamine. Model predictive controller are used to control each model subspace. 36 linear small-signal models were needed to span the entries space, but only the six models with the highest probability were used in the calculation to reduce computational time. The controller was robust and was compared to a previous multiple drug controller design. MMAC assumes that the patients response to a drug can be modeled in a finite number of ways. The absence of any system identification manoeuvre prior to the controller being initiated is one of the main attraction that the medical field sees in this controller.

**A Flexible Blood Flow Phantom Capable of Independently Producing Constant and Pulsatile Flow with a Predictable Spatial Flow Profile for Ultrasound Flow Measurement Validations [4]:**

This paper presents a flow phantom that can generate both pulsative and constant flow independently. A flexible blood flow phantom capable of generating predictable flow profiles under a wide variety of conditions was developed to validate the ultrasound time-domain correlation method of measuring blood flow. The purpose of the phantom is not to mimic the actual in vivo vessels but to generate flow with well-known flow properties. The phantom incorporates a computer controlled pulsative pump; it also supports multiple vessels with different sizes. This blood flow phantom was used to validate the UTDC blood flow measurement technique due to its ease of compatibility with different vessel geometries.

**Adaptive Control of Blood Pressure [2]:**

This paper discusses the development of a stochastic adaptive controller to control blood pressure during drug infusion. They also present an adaptive algorithm based on a minimum variance control law. A more advanced algorithm is also presented by including the rate of charge of the control signal in the performance measure. Both algorithms dynamic system is represented by an autoregressive-moving average. Stable control was achieved with both algorithms even with major circulatory changes. A smother control action is obtained with the one step ahead algorithm with less fluctuation

**Multiple-Model Adaptive Control of Blood Pressure Using Sodium Nitroprusside [5]:**

This paper presents a procedure to control arterial pressure using sodium nitroprusside with a multiple-model adaptive control. To achieve desired performance characteristics the controller includes pole-placement using state-variable feedback. The infusion delay time is removed by the Smith predictor to simplify the controller analysis and design. Zero steady state error is achieved using a PI controller. The robustness of this multiple model controller is shown by the results of the linear transfer function model simulator and the nonlinear pulsatile model. The controller was able to handel changes in the plant like large increase in the delay and doubling of the gain.

**A New Approach to Generate Arbitrary Pulsatile Pressure Wave Forms in Mechanical Circulatory Support Systems [1]:**

This paper presents a repetitive control algorithm as having application in the problem pulsative pressure and flow wave forms reproduction in rotary blood pumps. The algorithm was developed on a mock system. The model of the system was designed with repetitive control algorithm in mind. The experimental results show that the proposed method can reproduce pulsatile pressure patterns. This technique showed good tracking but some increase in convergence time because the motor has no breaking system and the unactuated response of the pump.

**A Model-Free Adaptive Control to a Blood Pump Based on Heart Rate [3]:**

In this paper a model free adaptive controller uses heart rate to regulate pump speed. In the circulatory system the body regulates heart rate (HR) to maintain constant arterial pressure (AP). The controller regulates pump speed based on the status of the circulatory system and a defined adjustable HR. To describe the mechanism and to test the controller a mathematic model of the cardiovascular-baroreflex

System that combined the intraaorta pump is used. The simulation results show that the HR is kept stable even with slight physical activity and failing of the left ventricle. The settling time of the controller is less than 5 seconds without static error or overshoot even with change in HR or the peripheral resistance disturbance.

# III. Model

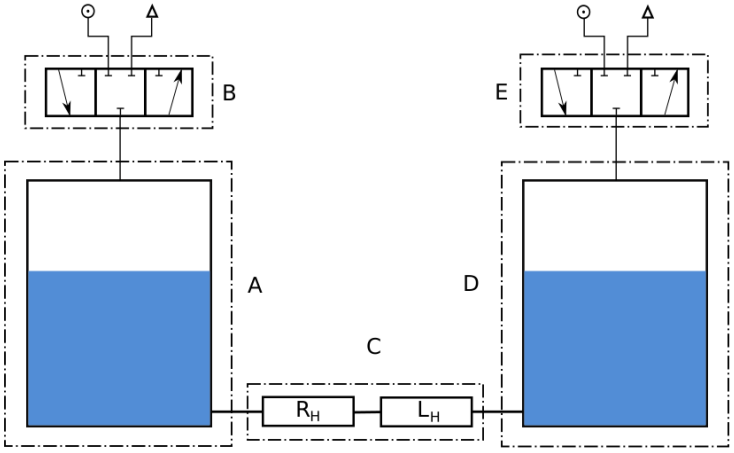


Fig. 1 Pneumatic damper diagram

Fig. 1 shows the pneumatic damper components. Subsystems A and B are the pressure chambers, B and E are the pneumatic electric valve, and C is the pipe system, which can be any desired hydraulic system.

## A. Pressure chamber

Water is free to travel from one chamber to another. The air entering the chamber increases its pressure and causes acceleration of the fluid in the hydraulic resistance and inductance.

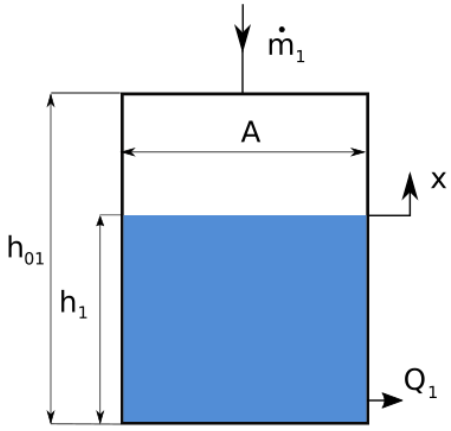


Fig. 2 Pressure Chamber

Compressed air enters the chamber with a mass flow rate $\dot{m}_1$ and temperature $T_A$. Let A be the cross section area of the tank and $h_0$ its height, which is constant, and $x$ is the height of the air-filled portion of the cylinder. The compressed air volume will be

$$V = x.A = (h_{01} - h_1)A \quad (1)$$

Air is assumed to behave as an ideal gas under adiabatic conditions, since the process is at low-temperature and low-pressure conditions, and it happens fast so no significant heat exchange will occur.

From the polytropic process condition, we have:

$$PV^n = const. \tag{2}$$

The ideal gas low gives:

$$PV = m\tilde{R}T \tag{3}$$

where $\tilde{R}$ is the air specific gas constant.

$$\tilde{R} = \frac{R_u}{M_{air}} = \frac{8.314}{28.97} = 287\,\frac{J}{kg.K} \tag{4}$$

where $R_u$ is the universal gas constant, and $M_{air}$ is the air molar mass.

The heat capacity at constant pressure,$C_P$, and heat capacity at constant volume, $C_V$, of an ideal gas are related as follows:

$$C_P - C_V = \tilde{R} \tag{5}$$

The heat capacity ratio is defined as

$$\gamma = \frac{C_P}{C_V} \tag{6}$$

which is equivalent to 1.41 at 20℃. $C_V$ can be written as

$$C_V = \frac{\tilde{R}}{\gamma - 1} \tag{7}$$

The energy balance of the chamber is given by the rate equation:

$$\dot{U} = \dot{H} + \dot{Q} - \dot{W} \tag{8}$$

where $\dot{U}$ is the internal energy rate of the gas, $\dot{H}$ is the enthalpy rate, $\dot{Q}$ is the heat rate, and $\dot{W}$ is the work rate. Since the process is assumed adiabatic, $\dot{Q}$ is canceled. Internal energy rate is given as

$$\dot{U} = \frac{d}{dt}(mC_V T) \tag{9}$$

Combining with (3) and (7), we get

$$\dot{U} = \frac{\dot{P}V + P\dot{V}}{\gamma - 1} \tag{10}$$

If the pressure variations are assumed not high enough to affect work rate, we get

$$\dot{W} = P_1\dot{V} \tag{11}$$

Enthalpy rate is

$$\dot{H} = \frac{d}{dt}(mC_P T) \tag{12}$$

From the energy balance equation we get

$$\dot{P_1} = \frac{\gamma \tilde{R}}{A} . \frac{\dot{m_1} T_{Af}}{(h_0 - h_1)} + \gamma \frac{P_1 \dot{h_1}}{(h_0 - h_1)} \tag{13}$$

$T_{Af}$ is the flow temperature.

The mass flow rate balance of the chamber gives:

$$\dot{h_1} = -\frac{1}{A} Q \tag{14}$$

where $Q$ is the flow exiting the first chamber.

**B. Valve dynamics**

The gas mass flow into the valve is a function of the valve opening. The valve is electrically controlled and it provide a continuous positioning. The properties of the air change while passing through the valve.

For a polytropic adiabatic process, the following equation holds:

$$P_A V_A^{\gamma} = P_S V_S^{\gamma} \tag{15}$$

Where $P_S$ and is the source (compressor) pressure, which is available from the compressor's pressure gage. $V_S$ is the volume of the air at the source, which is not used directly. Subscript A denotes the first pressure chamber A. Combining eq. (15) with eq. (3), we get

$$T_A = T_S \left(\frac{P_A}{P_S}\right)^{\frac{\gamma - 1}{\gamma}} \tag{16}$$

$T_S$ is the temperature at the source, which can be calculated based on the compressor specifications in continuous functioning.

The valve acts is two cases: pressurizing the chamber or depressurizing it. The general equation for the mass flow rate is given as

$$\dot{m} = u . c . P_u . \rho_0 . \sqrt{\frac{T_0}{T_u}} . \alpha \tag{17}$$

Where $u$ is the valve opening ratio (electrically controlled), $c$ and $b$ are valve coefficients, $\rho_0$ and $T_0$ are the air density and the air temperature at reference conditions. $P_u$and $T_u$are the upstream pressure and temperature respectively in bar and K.

$$\begin{aligned} c &= 0.45 l/sbar \\ b &= 0.21 \end{aligned} \tag{18}$$

$\alpha$ is defined as

$$\alpha = \sqrt{1 - \left(\frac{\frac{P_d}{P_u} - b}{1 - b}\right)^2} \quad for \ \frac{P_d}{P_u} > b \tag{19}$$

$$\alpha = 1 \text{ elsewhere}$$

$P_2$ is the downstream pressure in bar. Fig. 3 shows $\alpha$ explicitly for $b = 0.21$. It should be noticed that $\dot{m}_A$ would have the same behavior as $\alpha$ for a constant opening.

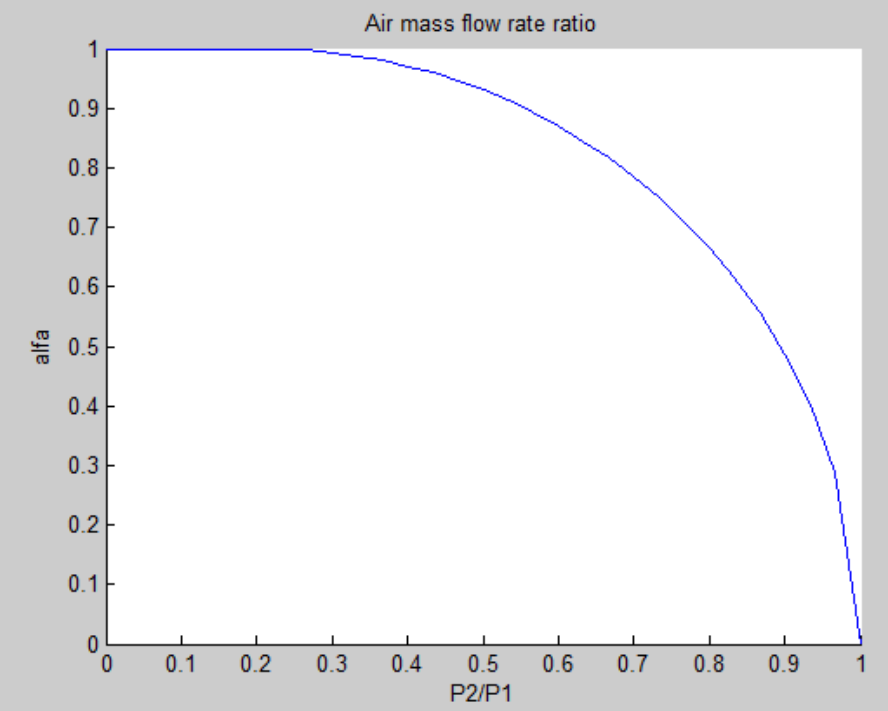


Fig. 3 plot of $\alpha$ vs $\frac{P_2}{P_1}$ for b=0.21

## C. Pipe line dynamics

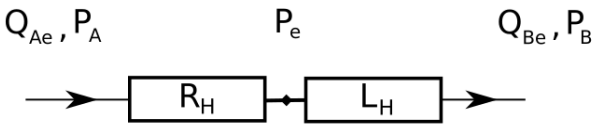


Fig. 4 Pipes schematic and parameters

Reynolds number for flow in pipe:

$$Re = \frac{Qd}{Av} \tag{20}$$

where $Q$ is the mean volumetric flow rate, $d$ is the diameter of the pipe, $A$ is the pipe cross , and $v = \mu/\rho$ is the kinematic viscosity of the fluid. The flow is laminar for $Re < 2300$, transient for $2300 < Re < 4000$, and turbulent for $Re > 4000$.

For a pipe diameter of 1 $cm$, the flow is laminar for a flow rate less than 18 $ml/s$, and turbulent for a flow rate above 31 $ml/s$.

The rate of blood pumped by one ventricle for an adult is about 5 $l/min$, or 83 $ml/s$, than for the specified system, an equivalent blood system would be in the turbulent state. However, for the test phase, signals of less than 20 $ml/s$ will be used, so the flow will be considered laminar.

The pressure drop for laminar flow is

$$P_1 - P_e = \frac{128.\mu.l}{\pi.d^4} \tag{21}$$

where $l$ is the pipe length. For turbulent flow the pressure drop is given by

$$P_1 - P_e = \frac{0.3164}{Re^{0.25}}.\frac{l}{d}.\frac{\rho}{2}.\frac{Q_1}{\left(\frac{\pi}{4}d^2\right)} \tag{22}$$

The pressure drop due to system inductance is given by the following equation:

$$P_e - P_2 = \frac{l.\rho}{A}.\dot{Q_1} \tag{23}$$

**D. System Dynamics summary**

$$\dot{P_1} = \frac{\gamma \tilde{R}\, T_f}{A_{ch}}.\frac{\dot{m_1}}{(h_0 - h_1)} + \gamma\frac{P_1\dot{h_1}}{(h_0 - h_1)}$$

$$\dot{P_2} = \frac{\gamma \tilde{R} T_f}{A_{ch}}.\frac{\dot{m_2}}{(h_0 - h_2)} + \gamma\frac{P_2\dot{h_2}}{(h_0 - h_2)}$$

$$\dot{h_1} = \frac{-1}{A_{ch}}Q$$

$$\dot{h_2} = \frac{1}{A_{ch}}Q$$

$$\dot{m_1} = u.C.P_{u1}.\rho_0.\sqrt{\frac{T_0}{T_{u1}}}.\alpha_1$$

$$\dot{m_2} = -u.C.P_{u2}.\rho_0.\sqrt{\frac{T_0}{T_{u2}}}.\alpha_2$$

$$P_1 - P_2 = \frac{128.\mu.l}{\pi.d^4}Q + \frac{l.\rho}{A_p}.\dot{Q}$$

## E. Nonlinear System Response

The model is tested for with a pulse signal, the response is shown in Fig. 5. This shows that the system model has a low damping, and a period of about 0.8 sec.

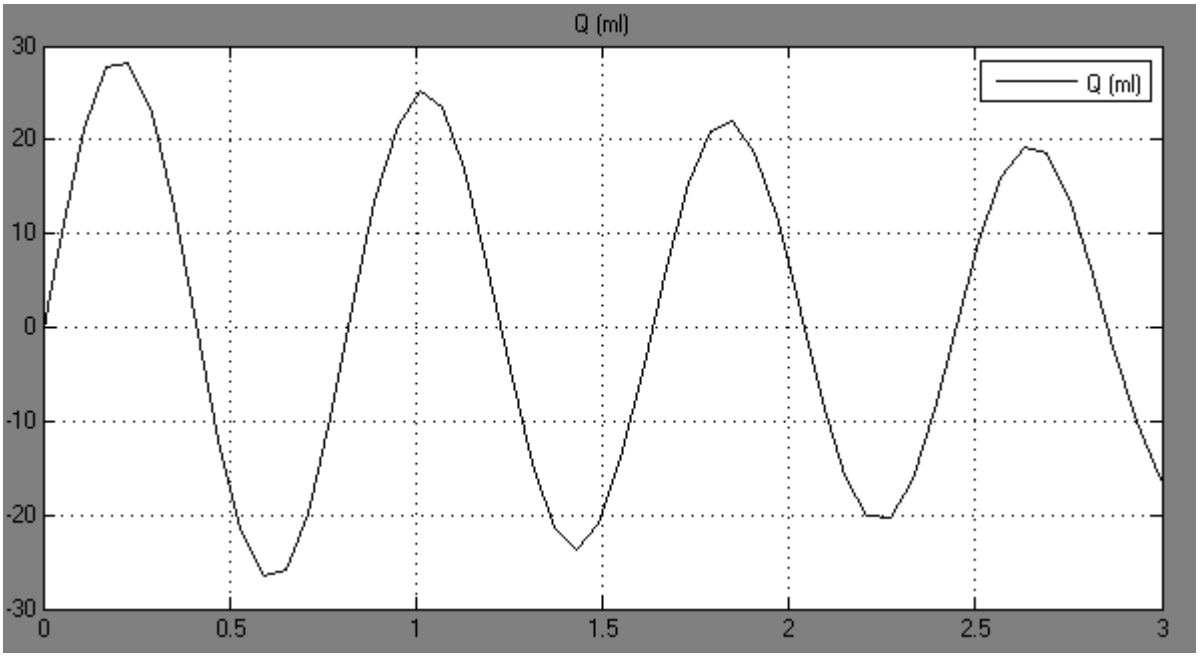


Fig. 5 Impulse response for the nonlinear model, the input is the valve opening position.

# IV. Linearization

## A. Working Point

The working point is chosen to be

$$\begin{gathered}\overline{P_1} = \overline{P_2} = 1.5\ bar \\ \overline{\dot{P}_1} = \overline{\dot{P}_2} = 0\ bar/s \\ \overline{X_1} = \overline{X_2} = \frac{h_0}{2} \\ \overline{\dot{X}_1} = \overline{\dot{X}_2} = 0\ m/s \\ \bar{Q} = 0\ m^3/s\end{gathered} \tag{24}$$

In order to linearize the system, Taylor series expansion for the first order is used. The linearized equation are then

$$\begin{gathered}\dot{P}_1 = c_1\,\dot{m}_1 - c_2\,\dot{X}_1 \\ \dot{P}_2 = c_1\,\dot{m}_2 + c_2\,\dot{X}_2\end{gathered}$$

$$\begin{gathered}\dot{m}_1 = c_3\,u(t) \\ \dot{m}_2 = -c_3\,u(t) \\ \dot{X}_1 = \frac{Q}{A} \\ \dot{X}_2 = -\frac{Q}{A}\end{gathered} \tag{25}$$

$$\dot{Q} = c_4 P_1 - c_4 P_2 - c_5 Q$$

where the parameters $c_i$ are defined as

$$c_1 = \frac{\gamma\,\tilde{R}\,T_f}{A\,\overline{X_1}}$$

$$\begin{gathered}c_2 = \frac{\gamma\,\overline{P_1}}{\overline{X_1}} \\ c_3 = \overline{P_1}\,C\,\rho_0\sqrt{\frac{T_0}{\overline{T_u}}}\sqrt{1-\left(\frac{\frac{\overline{P_d}}{\overline{P_u}}-b}{1-b}\right)^2} \\ c_4 = \frac{A_p}{l\,\rho} \\ c_5 = \frac{128\,\mu\,A_p}{\pi\,\rho\,d^4}\end{gathered} \tag{26}$$

## B. State Space Model

Considering the flowing linearized state space model:

$$\begin{aligned} \dot{X} &= AX + BU \\ Y &= CX + DU \end{aligned} \tag{27}$$

where A is the system matrix, B is the input matrix, C is the output matrix, D is the direct transition matrix, U is the input, and X is the states of the system.

The state space model is represented as follows

$$\dot{X} = \begin{Bmatrix} \dot{m}_1 \\ \dot{m}_2 \\ \dot{P}_1 \\ \dot{P}_2 \\ \dot{X}_1 \\ \dot{X}_2 \\ \dot{Q} \end{Bmatrix} = \begin{bmatrix} 0 & 0 & 0 & 0 & 0 & 0 & 0 \\ 0 & 0 & 0 & 0 & 0 & 0 & 0 \\ 0 & 0 & 0 & 0 & 0 & 0 & -c_2/A \\ 0 & 0 & 0 & 0 & 0 & 0 & c_2/A \\ 0 & 0 & 0 & 0 & 0 & 0 & 10^3/A \\ 0 & 0 & 0 & 0 & 0 & 0 & -10^3/A \\ 0 & 0 & c_4 & -c_4 & 0 & 0 & -c_5 \end{bmatrix} \begin{Bmatrix} m_1 \\ m_2 \\ P_1 \\ P_2 \\ X_1 \\ X_2 \\ Q \end{Bmatrix} + \begin{bmatrix} c_3 \\ -c_3 \\ c_1 c_3 \\ -c_1 c_3 \\ 0 \\ 0 \\ 0 \end{bmatrix} u \tag{28}$$

$$Y = \{Q\} = [0 \quad 0 \quad 0 \quad 0 \quad 0 \quad 0 \quad 1]X$$

## C. Output Controllability

The output controllability matrix is given as

$$W_{oc} = [CB \quad CAB \quad CA^2B \quad CA^3B \quad CA^4B \quad CA^5B \quad CA^6B] \tag{29}$$

which has the rank of one, and ensures that the system is output controllable.

# V. Reference model

## A. Continuous Time Domain

Based on the linearized state space system, the transfer function relating the pipe flow rate to the input signal is

$$G(s) = \frac{Q}{u} = \frac{2\,c_1 c_3 c_4}{s^2 + c_5 s + 2c_2 c_4 / A} \tag{30}$$

Which for the specified system parameters is equivalent to

$$G(s) = \frac{Q}{u} = \frac{2.497 \times 10^4}{s^2 + 0.3206 s + 56.51} \tag{31}$$

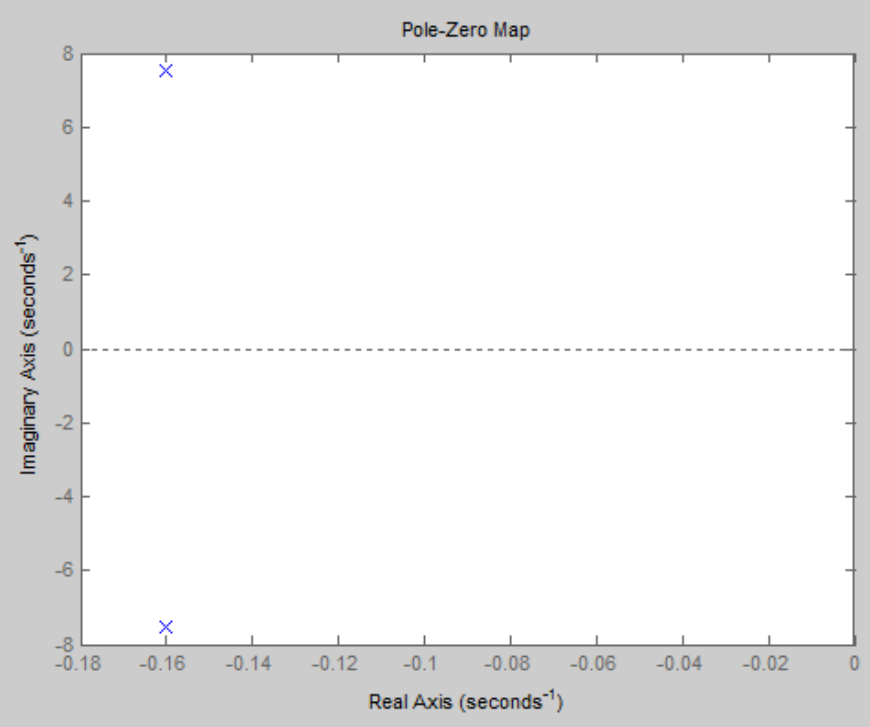


Fig. 6 Open loop Pole-Zero Map

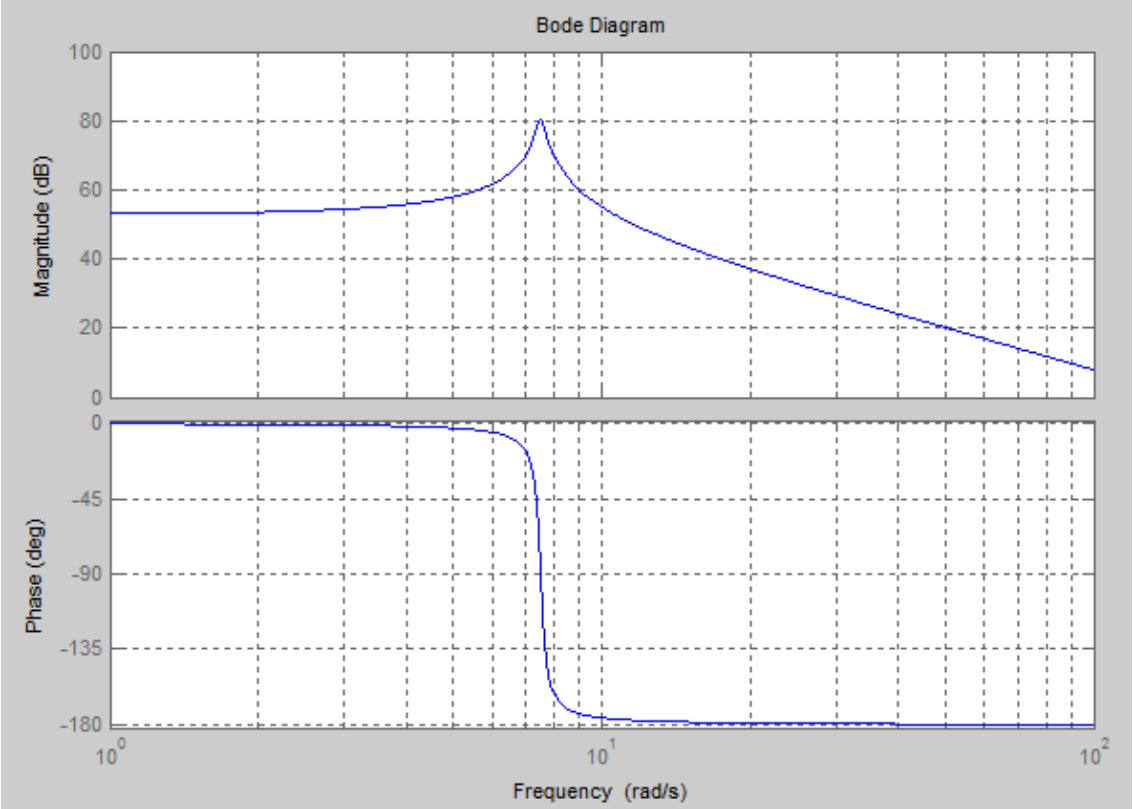


Fig. 7 Bode plot of the open loop transfer function

The system poles are always stable, but they have a very low damping. The desired model should keep close the the natural frequency of the system, while providing more damping to the system. The new second order system characteristics are assumed as

$$\begin{aligned} \zeta' &= 0.7 \\ \omega_n' &= 8\, rad/sec \end{aligned} \tag{32}$$

The new model is defined as

$$G_m(s) = \frac{b_m}{s^2 + a_{m1}s + a_{m2}} \tag{33}$$

where

$$\begin{aligned} a_{m1} &= 2\zeta'\omega_n' \\ a_{m2} &= \omega_n'^2 \\ b_m &= a_{m2}\ (for\ unity\ s.s.\ gain) \end{aligned} \tag{34}$$

The closed loop transfer function becomes:

$$H(s) = \frac{Q(t)}{u(t)} = \frac{64}{s^2 + 11.2\, s + 64} \tag{35}$$

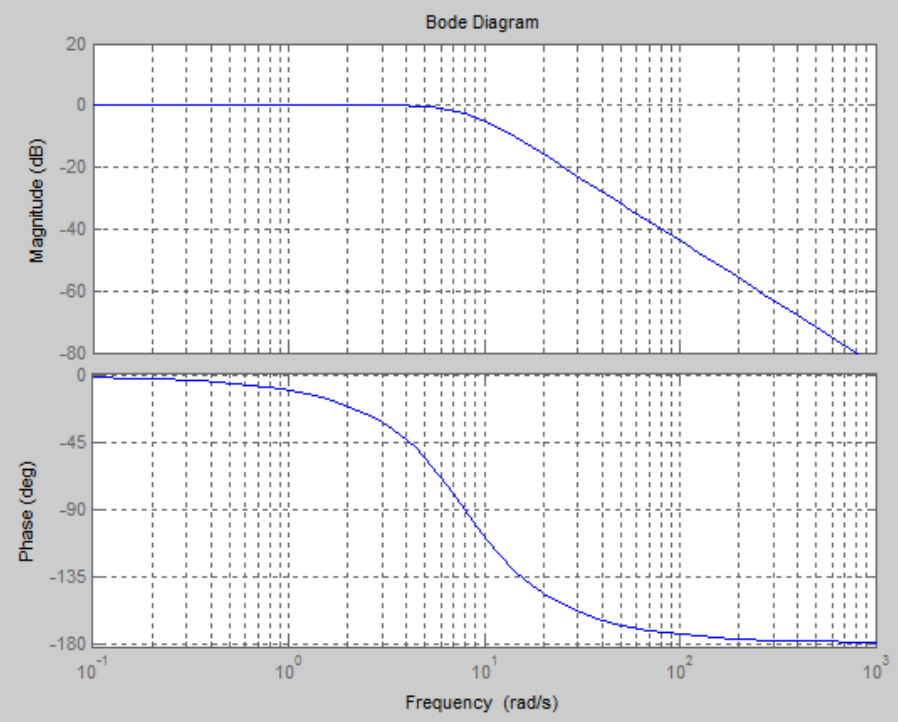


Figure 1 Closed loop bode plot

## B. Discrete Time Domain

The discrete time transfer function for a sampling period $T_{samp} = 0.01s$ is given as

$$H(z) = \frac{Q(t)}{u(t)} = \frac{1.247\,z + 1.245}{z^2 - 1.991\,z + 0.9968} \tag{36}$$

The zero-pole plot is given by Fig. 8. The zero is stable, however, it is very close to the unity circle, so it is not well damped and controller design with zero cancelation approach is not recommended since it will add ringing to the control signals.

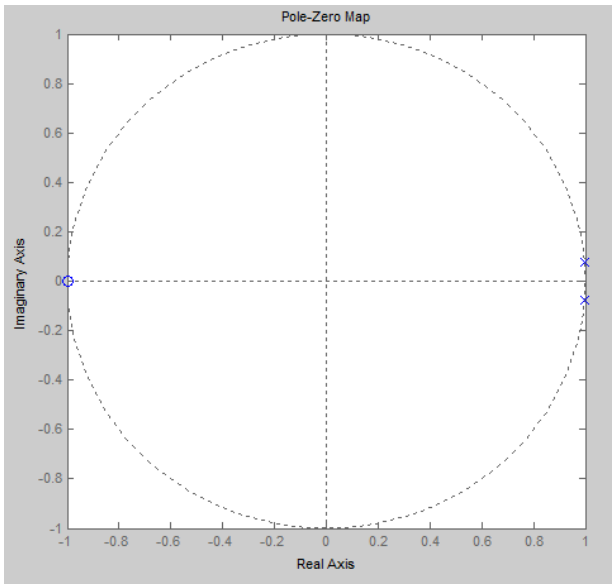


Fig. 8 Zero-pole plane for discrete transfer function

## C. Linear system response

The impulse response of the linearized system is shown in Fig. 9, and it shows similar performance of the nonlinear model, which proves the validity of the linearization.

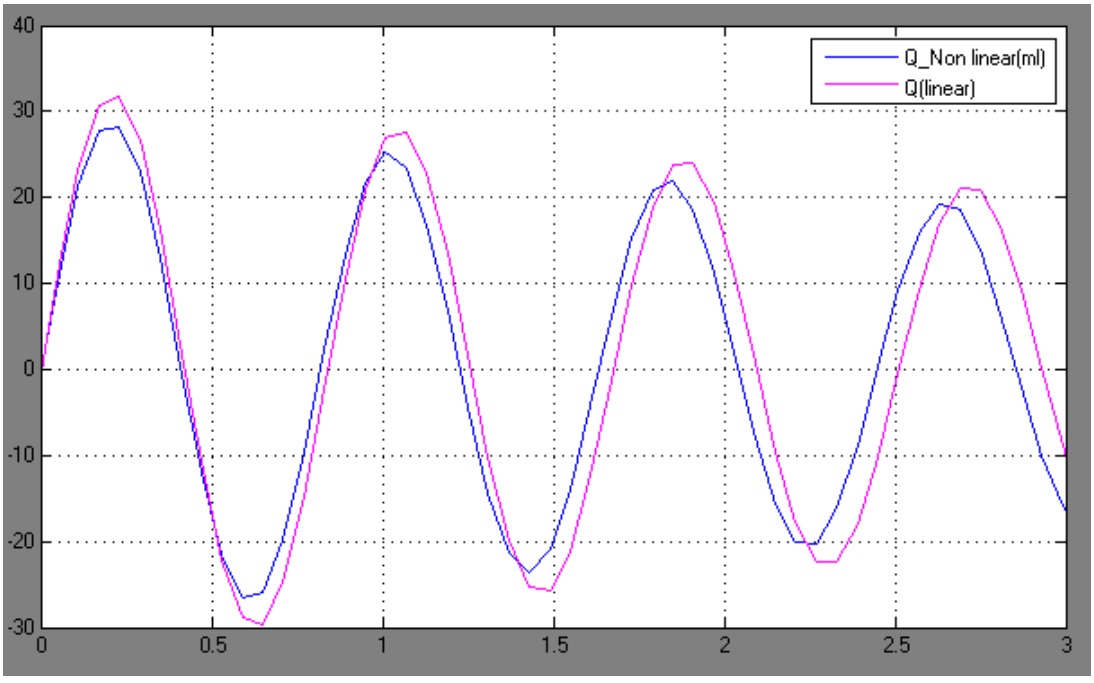


Fig. 9 Impulse response of the linear system compared to the nonlinear one

## VI. Controller Design

The control law used for the system is

$$Ru(t) = Tu_c(t) - Sy(t) \tag{37}$$

Which represents a negative feedback and a feed-forward.

The closed loop system can described as:

$$\begin{aligned} y(t) &= \frac{BT}{AR + BS} u_c(t) \\ u(t) &= \frac{AT}{AR + BS} u_c(t) \end{aligned} \tag{38}$$

The closed loop characteristic polynomial is given as:

$$AR + BS = A_c \tag{39}$$

Factorizing $B$ as

$$B = B^+ B^- \tag{40}$$

Where $B^+$ is monic and represents the stable and well damped zeros, and $B^-$ represents the unstable or poorly damped zeros.

### A. Continuous Time Domain

The solution is based on the eq.(33) and (35). Solving eq.(39) for

$$\begin{aligned} B^+ &= 1 \\ B^- &= B \end{aligned} \tag{41}$$

The degrees of $R, S, T$ and $A_o$ are chosen to be one, and $A_c = A_o A_m B^+$. Solving eq. (39) for $R$ and $S$, we get

$$\begin{aligned} r_1 &= a_0 + a_{m1} - a\_1 \\ s_0 &= (a_{m1} a_0 + a_{m2} - a_1 r_1 - a_2)/b_0 \\ s_1 &= (a_{m2} a_0 - a_2 r_1)/b_0 \end{aligned} \tag{42}$$

And $T$ is given as

$$T = B'_m A_o = t_0 s + t_1 \tag{43}$$

Where $t_0$ and $t_1$ are calculated as

$$\begin{aligned} t_0 &= \frac{b_m}{b_0} \\ t_1 &= \frac{b_m a_0}{b_0} \end{aligned} \tag{44}$$

## B. Discrete Time Domain

The solution is based on the eq.(36).

### Model-following without Zero Cancellation

For the case when the zero in not cancelled, which is the true case, we chose

$$\begin{aligned} B^+ &= 1 \\ B^- &= B \end{aligned} \tag{45}$$

The degrees of $R, S, T$ and $A_o$ are chosen to be one, and $A_c = A_o A_m B^+$. Solving eq. (39) for $R$ and $S$, we get

$$\begin{aligned} r_1 &= \frac{a_0 a_{m2} b_0^2 + (a_2 - a_{m2} - a_0 a_{m1}) b_0 b_1 + (a_0 + a_{m1} - a_1) b_1^2}{b_1^2 - a_1 b_0 b_1 + a_2 b_0^2} \\ s_0 &= \frac{b_1 (a_0 a_{m1} - a_2 - a_{m1} a_1 + a_1^2 + a_{m2} - a_1 a_0)}{b_1^2 - a_1 b_0 b_1 + a_2 b_0^2} \\ &\quad + \frac{b_0 (a_{m1} a_2 - a_1 a_2 - a_0 a_{m2} + a_0 a_2)}{b_1^2 - a_1 b_0 b_1 + a_2 b_0^2} \\ s_1 &= \frac{b_1 (a_1 a_2 - a_{m1} a_2 + a_0 a_{m2} - a_0 a_2)}{b_1^2 - a_1 b_0 b_1 + a_2 b_0^2} \\ &\quad + \frac{b_0 (a_2 a_{m2} - a_2^2 - a_0 a_{m2} a_1 + a_0 a_2 a_{m1})}{b_1^2 - a_1 b_0 b_1 + a_2 b_0^2} \end{aligned} \tag{46}$$

And $T$ is given as

$$T = t_0 A_o \tag{47}$$

Where $t_0$ is calculated as

$$t_0 = \frac{1 + a_{m1} + a_{m2}}{b_0 + b_1} \tag{48}$$

The observer polynomial $A_o$ is

$$A_o = q + a_o \tag{49}$$

With $a_o = 0$.

The input signal is fed to the system model in discrete time domain as

$$u(t) = [-r_1 u(t-1) + t_0 u_c(t) - s_0 y(t) - s_1 y(t-1)] \tag{50}$$

### Model-following with Zero Cancellation

The case considering zero cancelation will be implemented for demonstration. We choose

$$B^+ = q + \frac{b_1}{b_0}$$
$$B^- = b_0$$
$$B_m^{'} = \frac{b_{m0}q}{b_0}$$

Solve the Diophantine equation

$$AR' + b_0S = A_0A_m$$

where $A_0$ = R' =1

$$(q^2 + a_1q + a_2).1 + b_0(s_0q + s_1) = q^2 + a_{m1}q + a_{m2}$$

Equating coefficients of equal power of q:

$$s_0 = \frac{a_{m1} - a_1}{b_0}$$
$$s_1 = \frac{a_{m2} - a_2}{b_0}$$

As a result, the controller polynomials are:

$$R = B^+ = q + \frac{b_1}{b_0}$$
$$S = s_0q + s_1$$
$$T = A_0B'_m = \frac{b_{m0}q}{b_0}$$

Even though the process has a stable zero, it is still not well damped. However, we will try to use it with our self-tuning regulator for testing purposes.

The input signal is fed to the system model in discrete time domain as

$$u(t) = [-r_1u(t-1) + t_0u_c(t) - s_0y(t) - s_1y(t-1)] \quad (51)$$

# VII. Adaptive Control Approach

## A. MRAC

An output feedback MRAC law is considered. By calculating $G(j\omega)$, it is proved that it is not positive real, so we are seeking to use I/O stability theory the find a parameter adaptation law for a stable adaptive system.

### Adaptive controller Design

The error model is given as

$$e(t) = \frac{b_0}{A_o A_m}\big(Ru(t) + Sy(t) - Tu_c(t)\big) \tag{52}$$

But $\frac{b_0}{A_o A_m}$ is not SPR so we introduce the filtered error

$$e_f(t) = \frac{b_0 Q}{A_o A_m}\left(\frac{R}{P}u(t) + \frac{S}{P}y(t) - \frac{T}{P}u_c(t)\right) \tag{53}$$

$Q\ and\ P$ are selected as

$$\begin{aligned} Q &= A_o A_m \\ P_1 &= A_m \\ P_2 &= A_o \\ P &= P_1 P_2 \end{aligned} \tag{54}$$

Then $e_f(t)$ reduces to $e_f(t) = e(t) = y(t) - y_m(t)$

Q must satisfy $G_1(s) = \frac{b_0 Q}{A_o A_m}$ being SPR, and P can be any stable polynomial as long as $\frac{Q}{P}$ is causal. Doing the following separation:

$$\begin{aligned} \frac{R}{P} &= \frac{1}{P_1} + \frac{R'}{P_1 P_2} \\ R' &= r_1 - a_o \end{aligned} \tag{55}$$

Then $e_f$ becomes

$$\begin{aligned} e_f(t) &= \frac{b_0 Q}{A_o A_m}\left(\frac{1}{P_1}u(t) + \frac{R'}{P}u(t) + \frac{S}{P}y(t) - \frac{T}{P}u_c(t)\right) \\ &= G_1(s)\left(\frac{1}{P_1}u(t) + \varphi^T(t)\theta^0\right) \end{aligned} \tag{56}$$

To reduce the error to zero, the input signal $u(t)$ is chosen as

$$u(t) = -P_1(s)[\varphi^T(t)\theta^0] \tag{57}$$

However this equation can mot be implemented since it include higher derivatives of $\theta(t)$, so we introduce

$$u(t) = -\theta^T(t)P_1[\varphi^T(t)] \tag{58}$$

The augmented error is defined as

$$\varepsilon = e_f + G_1(s)\eta \tag{59}$$

where

$$\eta = -\left(\frac{1}{P_1}u(t) + \varphi^T(t)\theta(t)\right) \tag{60}$$

$\varphi(t)\ and\ \theta(t)$ are found as

$$\varphi^T(t) = \frac{1}{P}[u(t) \quad sy(t) \quad y(t) \quad -su_c(t) \quad -u_c(t)]$$
$$\theta^T(t) = [r_1' \quad s_0 \quad s_1 \quad t_0 \quad t_1] \tag{61}$$

The parameter adjustment law is given as

$$\dot{\theta}(t) = \gamma\varphi(t)\varepsilon(t) \tag{62}$$

But this law cannot be implemented since it includes an unknown ($b_0$). To overcome this problem, $b_0$ is estimated. Introducing the following filtered values:

$$u_f(t) = \frac{Q}{A_o A_m P_1}u(t)$$
$$\varphi_f(t) = \frac{Q}{A_o A_m}\varphi(t) \tag{63}$$

The estimated filtered error is then

$$\hat{e}_f = \hat{b}_0(u_f(t) + \varphi^T(t)\theta(t)) \tag{64}$$

The augmented effort becomes

$$\varepsilon_p = e_f - \hat{e}_f \tag{65}$$

$b_0$ is estimated as

$$\dot{\widehat{b_0}} = \gamma_1\left(u_f + \varphi_f^T(t)\theta(t)\right)\varepsilon_p \tag{66}$$

Finally, the normalized parameter adaptation law is given as

$$\dot{\theta}_N(t) = \frac{\gamma_2\varphi_f(t)\varepsilon_p}{\alpha + \varphi_f^T(t)\gamma_2\varphi_f(t)} \tag{67}$$

Where $\gamma_1, \gamma_2, and\ \alpha$ are calculated as follows:

$$\gamma_1 = \frac{10^{2.5}}{u_{c,max}}$$

$$\gamma_2 = \gamma_1/\widehat{b_0}$$

$$\alpha = 1/\gamma_1$$

There relations where found by iteration, and have gave the best performance for the controller.

The observer coefficient was found best to be at $a_0 = 1.5$.

## B. Self-Tuning Regulator

### Indirect Self-Tuning Regulator, No Zero Cancelation Case

Model parameters, i.e. $a_1, a_2, b_0 \; and \; b_1$, are estimated using the recursive least square method with exponential forgetting.

$$\begin{gathered} \hat{\theta}(t) = \hat{\theta}(t-1) + K(t)\left(y(t) - \varphi^T(t)\hat{\theta}(t-1)\right) \\ K(t) = P(t)\varphi(t) = P(t-1)\varphi(t)\left(\lambda I + \varphi^T(t)P(t-1)\varphi(t)\right)^{-1} \\ P(t) = \left(I - K(t)\varphi^T(t)\right)P(t-t)/\lambda \end{gathered} \tag{68}$$

The parameters vector is selected as

$$\hat{\theta}^T(t) = [\hat{a}_1 \quad \hat{a}_2 \quad \hat{b}_0 \quad \hat{b}_1] \tag{69}$$

And the regressors' vector is chosen as

$$\varphi^T(t) = [-y(t-1) \quad -y(t-2) \quad u(t-1) \quad u(t-2)] \tag{70}$$

The estimated parameters are used to calculate the controller parameters: $r_1, s_0, s_1, and \; t_0$.

### Direct Self-Tuning Regulator, Zero Cancelation Case

First, we estimate the coefficients of R and S using recursive least squares method of the model

$$y(t) = R^* u_f(t-1) + S^* y_f(t-1) \tag{71}$$

Where $u_f(t) = \frac{1}{A_m^*}u(t)$ and $y_f(t) = \frac{1}{A_m^*}y(t)$, and $y(t) = \varphi(t-1)\theta(t)$ .The regressors and the parameters vector are given as

$$\begin{gathered} \theta^T(t) = [r_0 \quad r_1 \quad s_0 \quad s_1] \\ \varphi^T(t-1) = [u_f(t-1) \quad u_f(t-2) \quad y_f(t-1) \quad y_f(t-2)] \end{gathered} \tag{72}$$

After that, we use the estimated parameters to compute the input signal from the control law

$$u(t) = \frac{1}{\theta(1)}[-\theta(2)u(t-1) + \hat{t}_0 u_c(t) - \theta(3)y(t) - \theta(4)y(t-1)]$$

with

$$\hat{t}_0 = 1 + a_{m1} + a_{m2}.$$

## VIII. Simulation Results

### A. MRAC, Output Feedback

Fig. 10, Fig. 11, and Fig. 12 show a good parameters convergence, but they suffers from a small ringing. Fig. 13 shows a good model following with a small error. Fig. 14 shows the input signal to the actuator for a desired patter of a square signal between [-10,10].

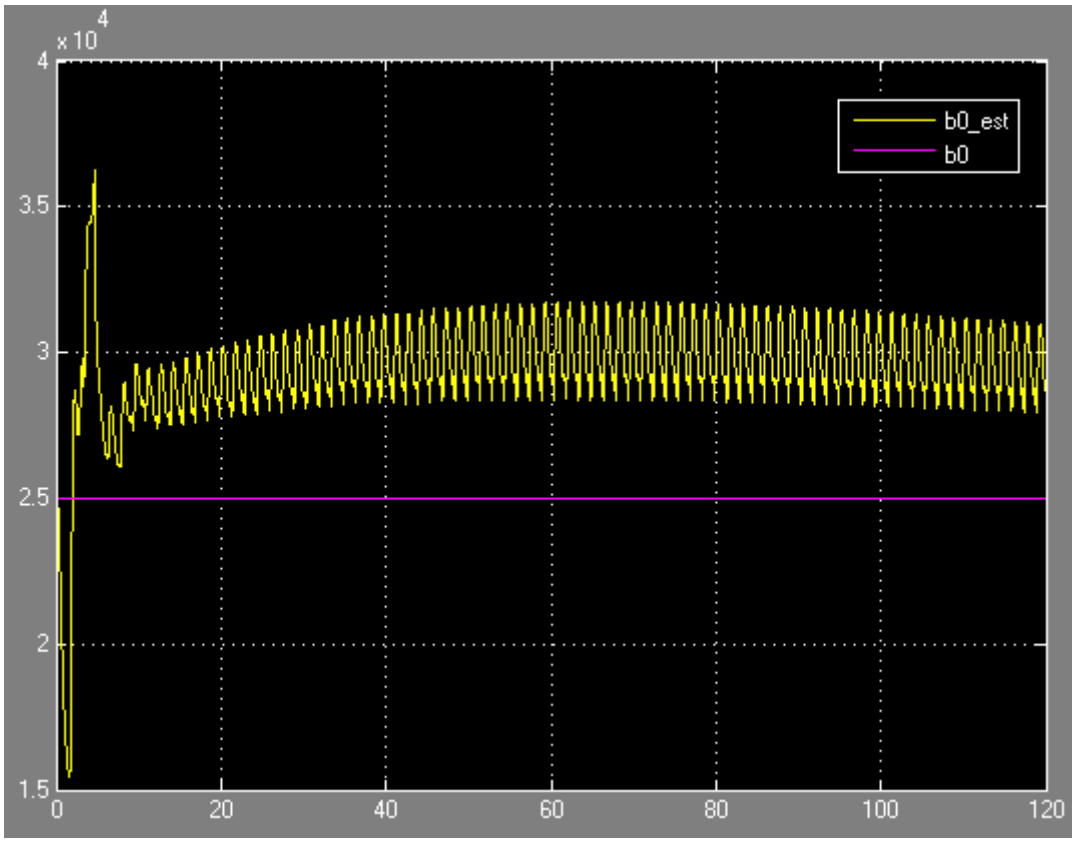


Fig. 10 $b_0$ parameter estimate in the MRAC model

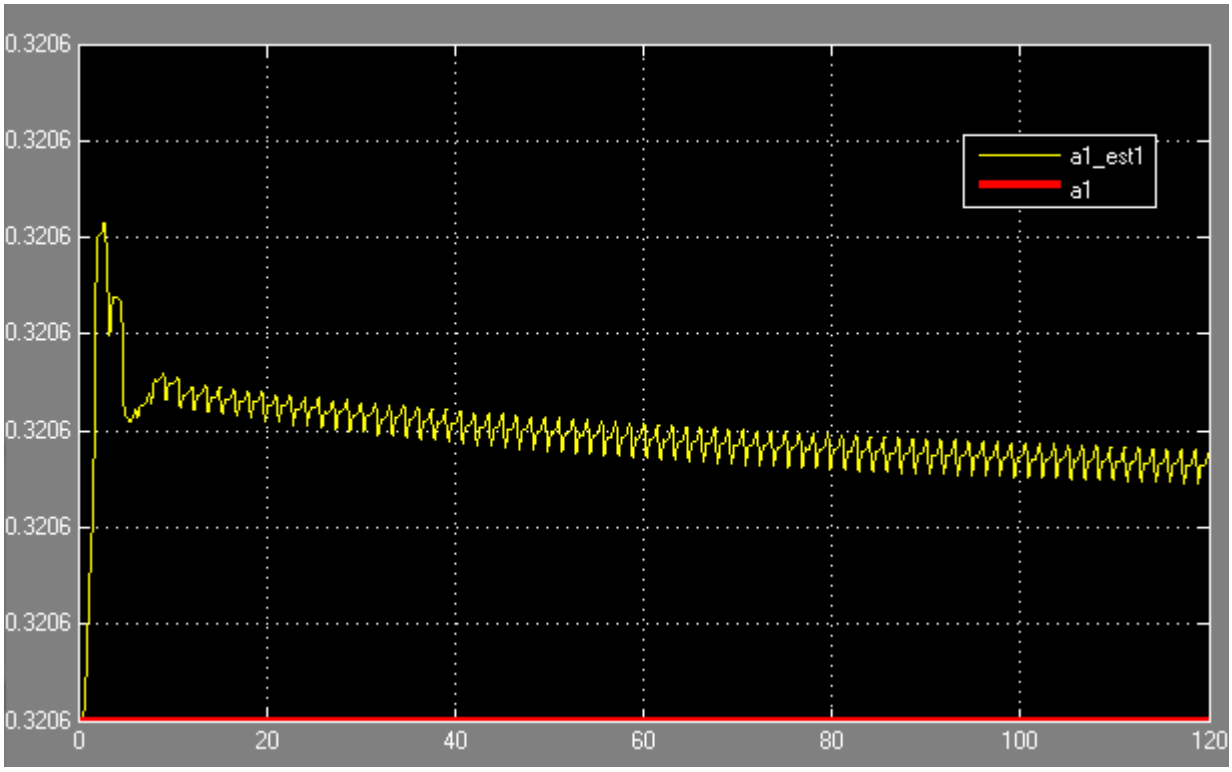


Fig. 11 $a_1$ parameter estimate in the MRAC model

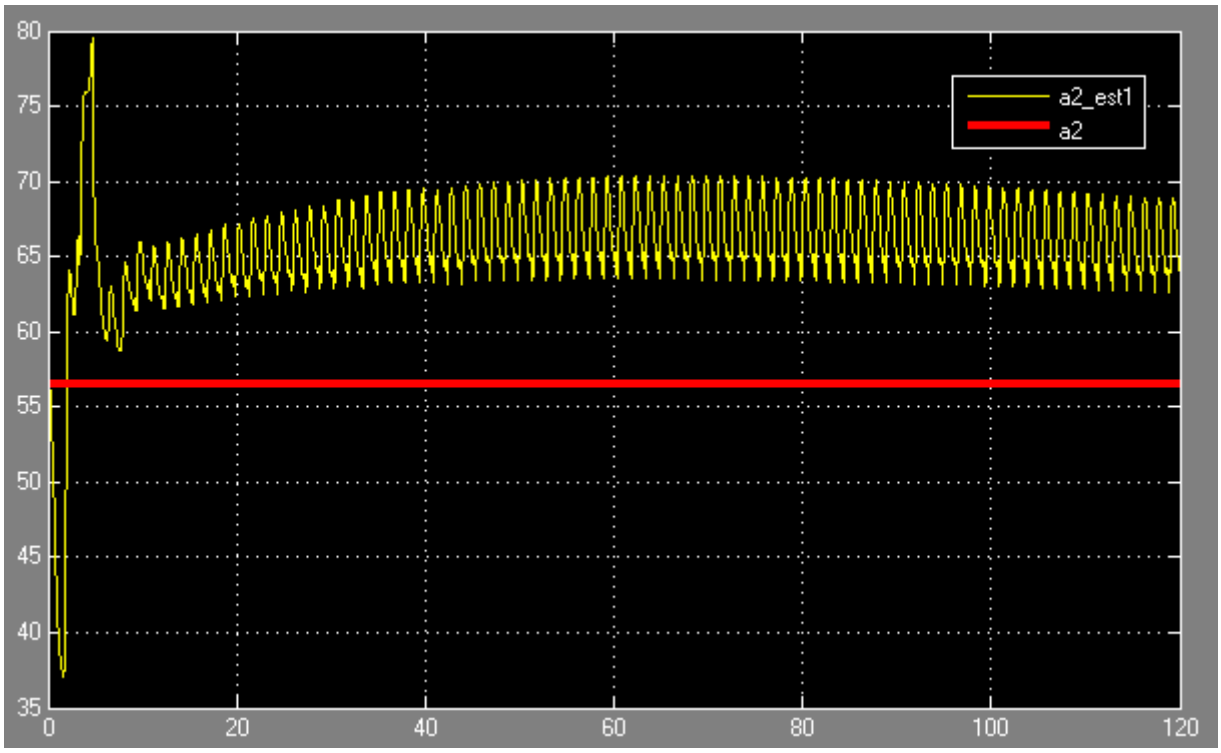


Fig. 12 $a_2$ parameter estimate in the MRAC model

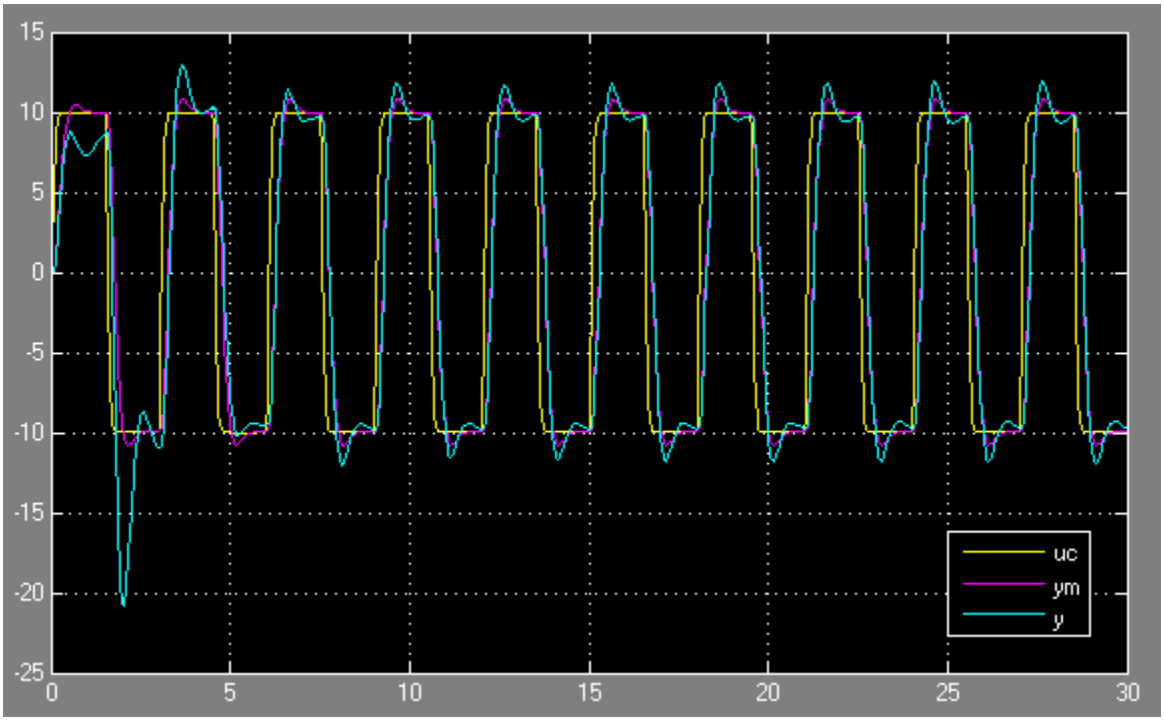


Fig. 13 Output y(t) compared to the reference model for an input square signal.

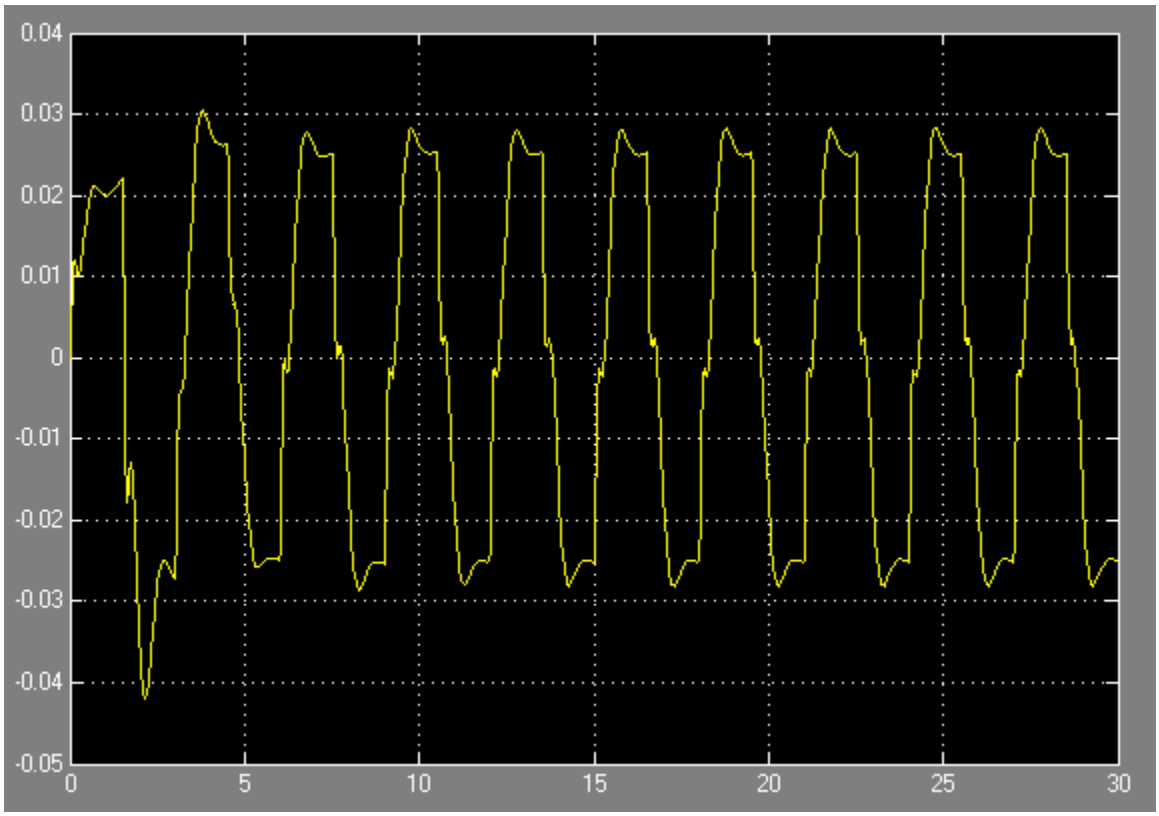


Fig. 14 Input signal u(t) for a square control signal [-10,10].

## B. Indirect Self-Tuning Regulator, No Zero Cancelation Case

In order for the estimated parameters to converge to their true values, the input signal need to be persistently exciting of order four. This is achieved with a square signal with a period of at most 9 $s$.

The controller is tested on the nonlinear model of the system. The parameters of the linearized model are slightly different from non-linear one. This is demonstrated with the values of $\hat{b}_0 \; and \; \hat{b}_1$. However, the values of $\hat{a}_1 and \; \hat{a}_2$ are almost identical to their linear values.

Fig. 17 shows the values when the input signal is a square signal with period of 3 $sec$, and an amplitude of 10, and initial values of the parameters as follows:

$$theta_{init} = 0.8.\,[\,a_1 \; a_2 b_0 \; b_1]$$

The control signal is ringing free, as shown in Fig. 18 and has an order of less than 0.1, which requires the actuator, i.e. the pneumatic valve, to have a very high resolution.

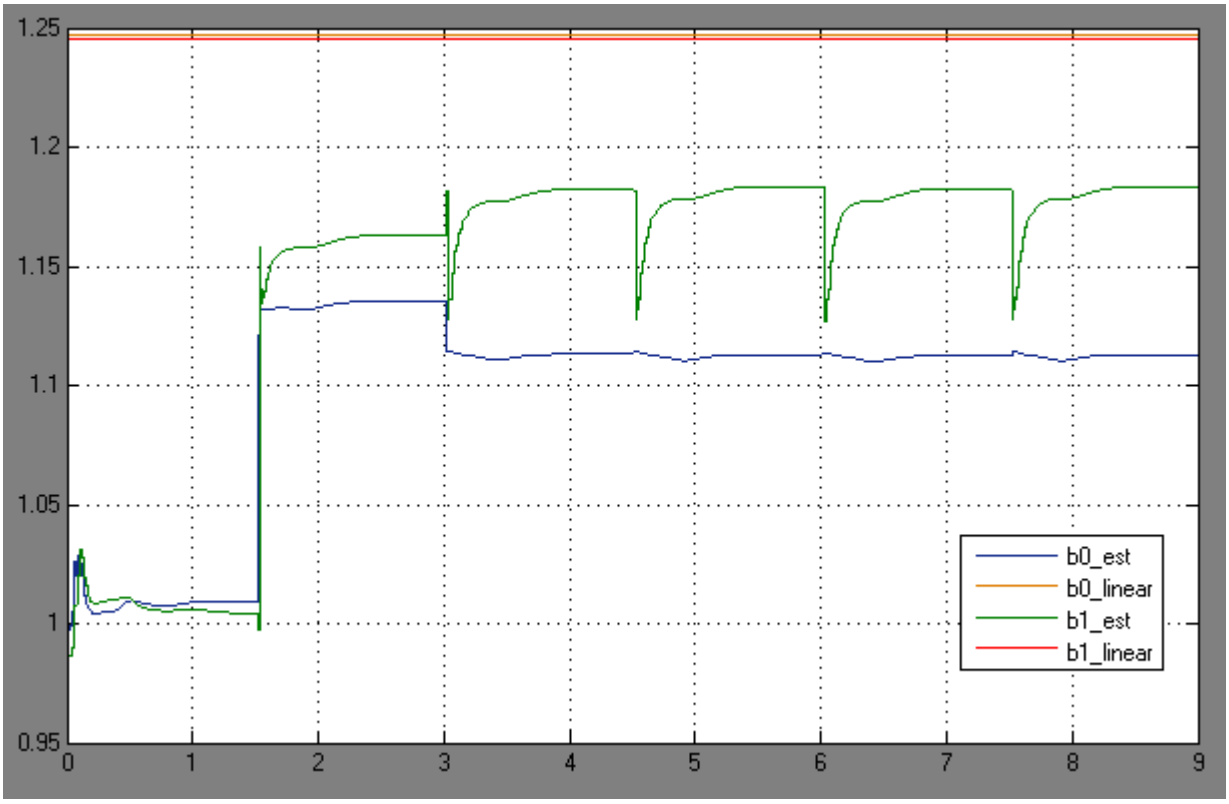


Fig. 15 B Parameters estimation for a square signal with a period of 3 sec.

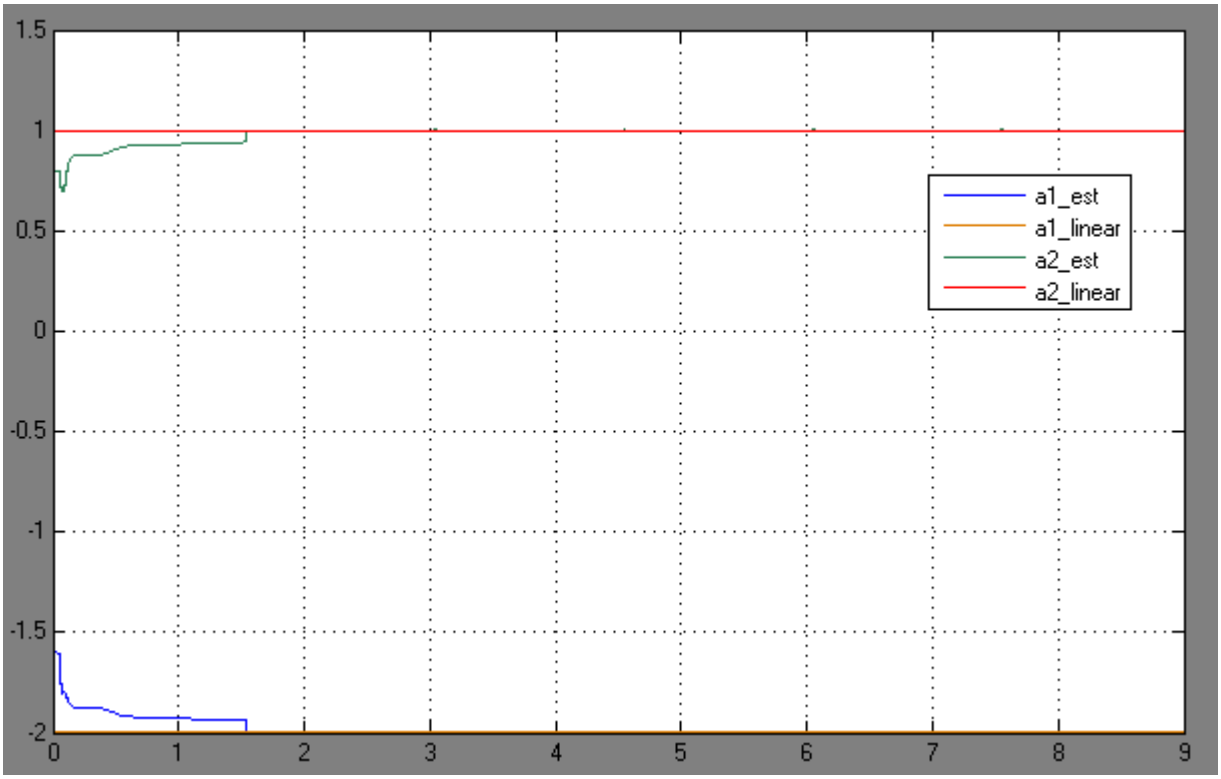


Fig. 16 A Parameters estimation for a square signal with a period of 3 sec.

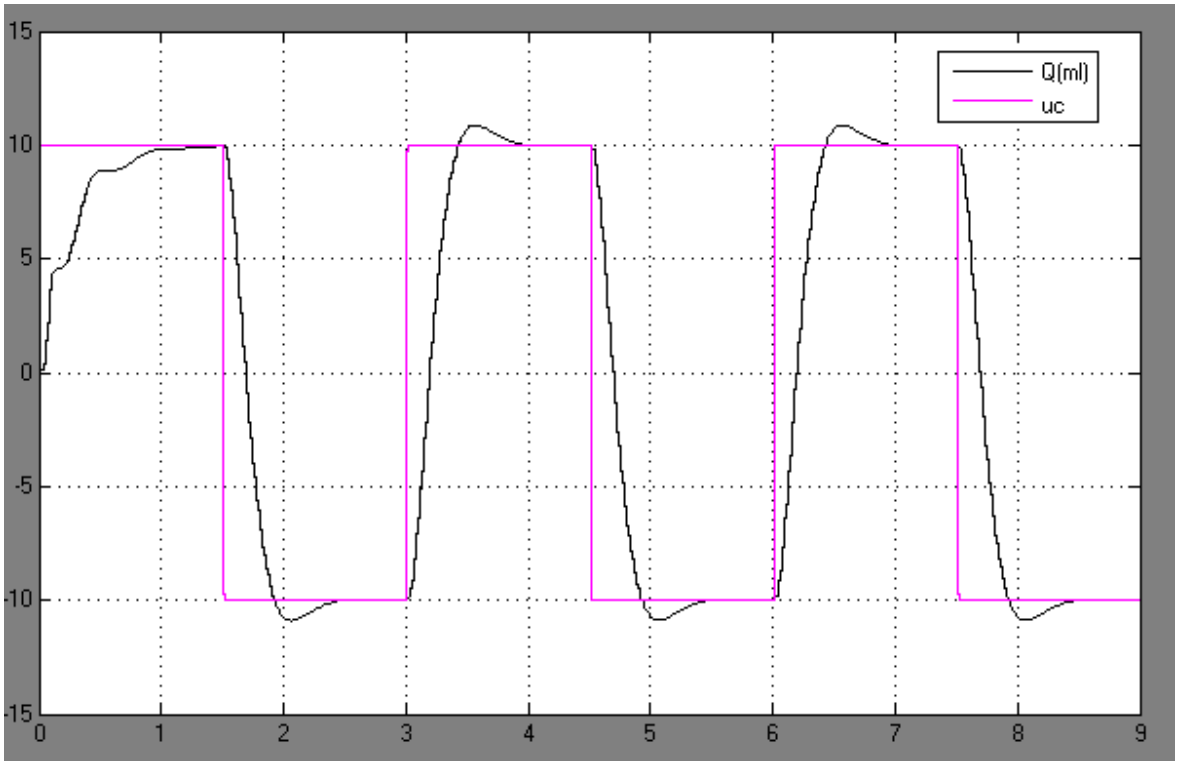


Fig. 17 System response for a square signal [-10,10] with a frequency of period of 3 *sec*.

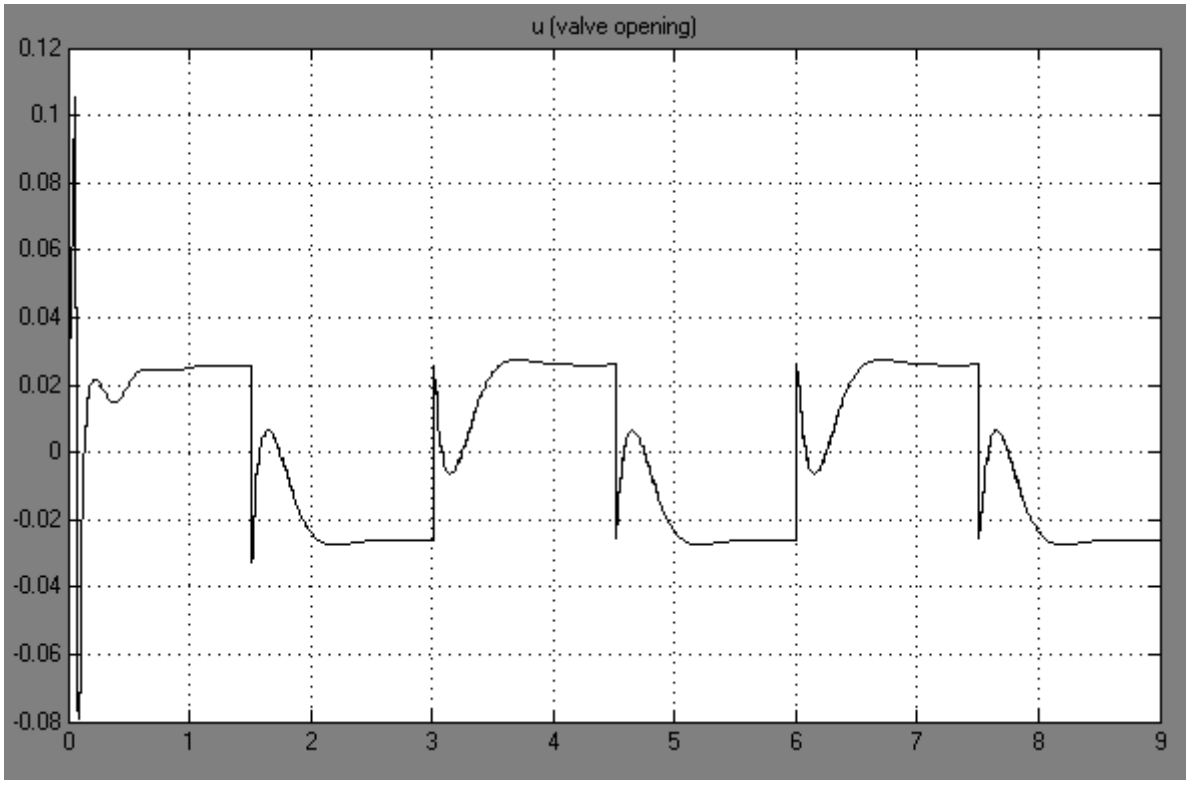


Fig. 18 Input signal for a control square signal [-10,10] with a frequency of period of 3 sec.

### C. Comparison between ISTR and simple controller

The amount of water inside the chambers is constant, so if the fluid move only in one direction the system will drift away from working point, i.e. at $h = H/2$, and that will cause a change in the system parameter. In such a case, the adaptive controller proved a better performance showing no sensitivity to the change the fluid height (Fig. 19). As depicted in Fig. 20, the error in the case of simple controller will keep increasing while the water level inside the pressure chambers is changing (Fig. 21). The adaptive system keeps changing the controller parameters based on the estimated values of the system parameters, which is shown in Fig. 22.

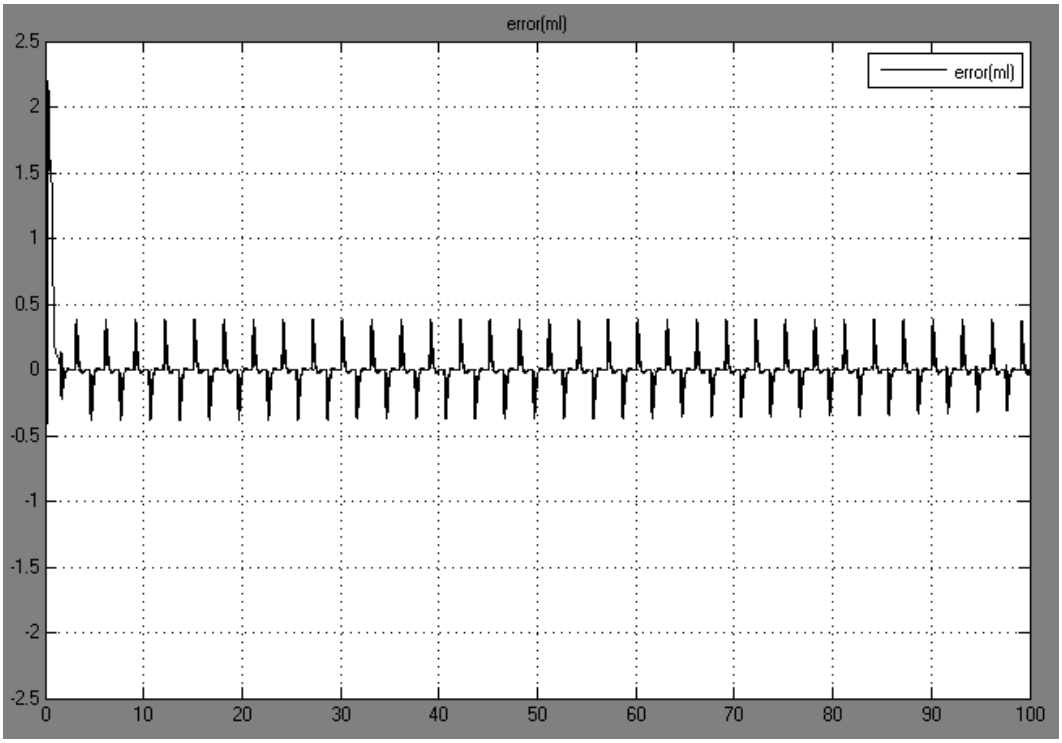


Fig. 19 Output error based on the reference model for a [0,10] square signal for the *adaptive* controller with the nonlinear model.

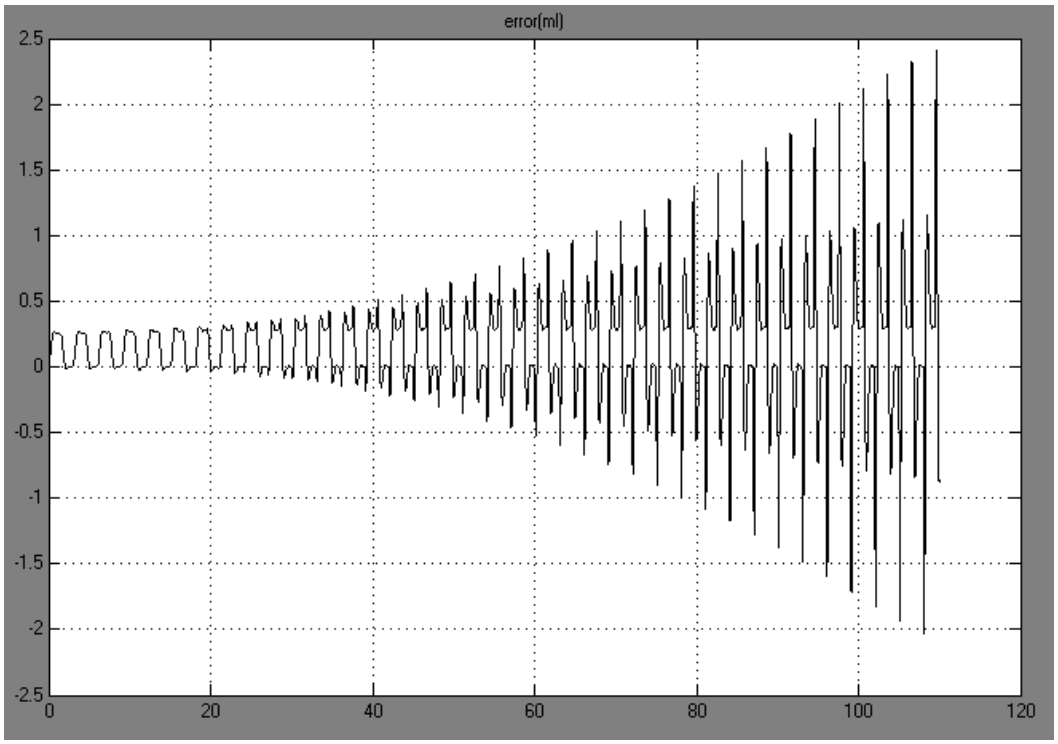


Fig. 20 Output error based on the reference model for a [0,10] square signal for the *simple* controller with the nonlinear model.

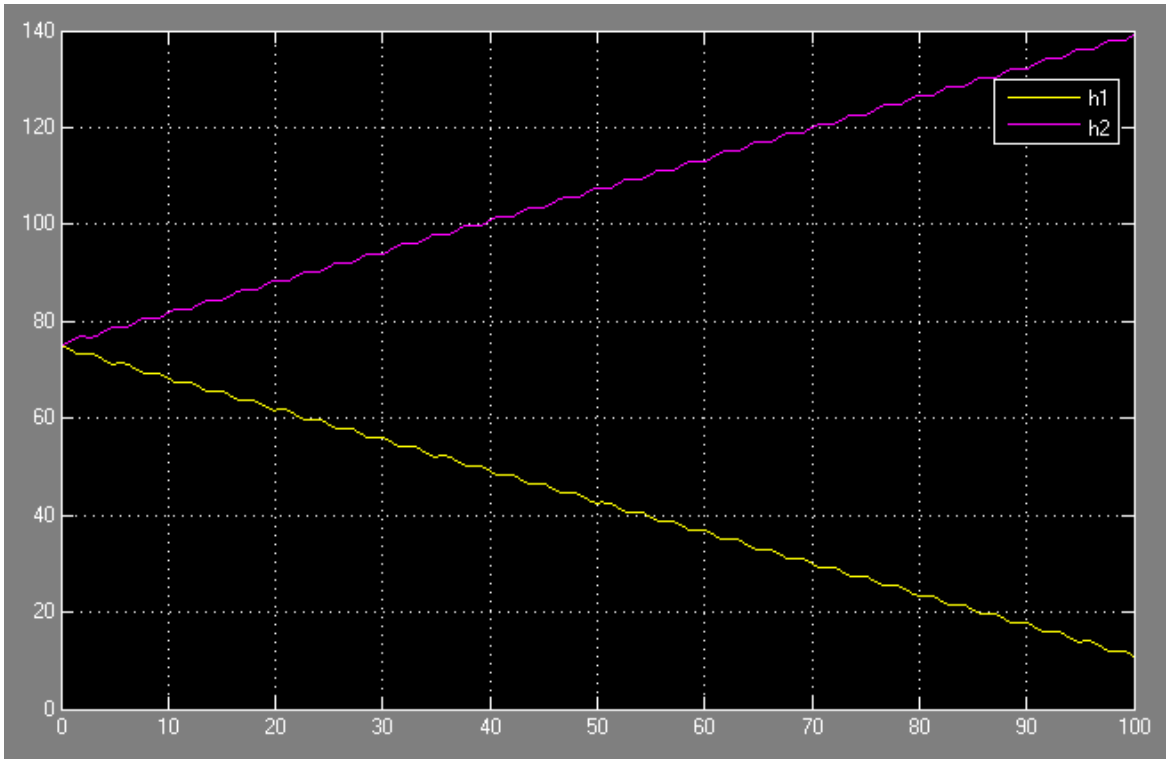


Fig. 21 Water level inside the pressure chamber model for a [0,10] square signal.

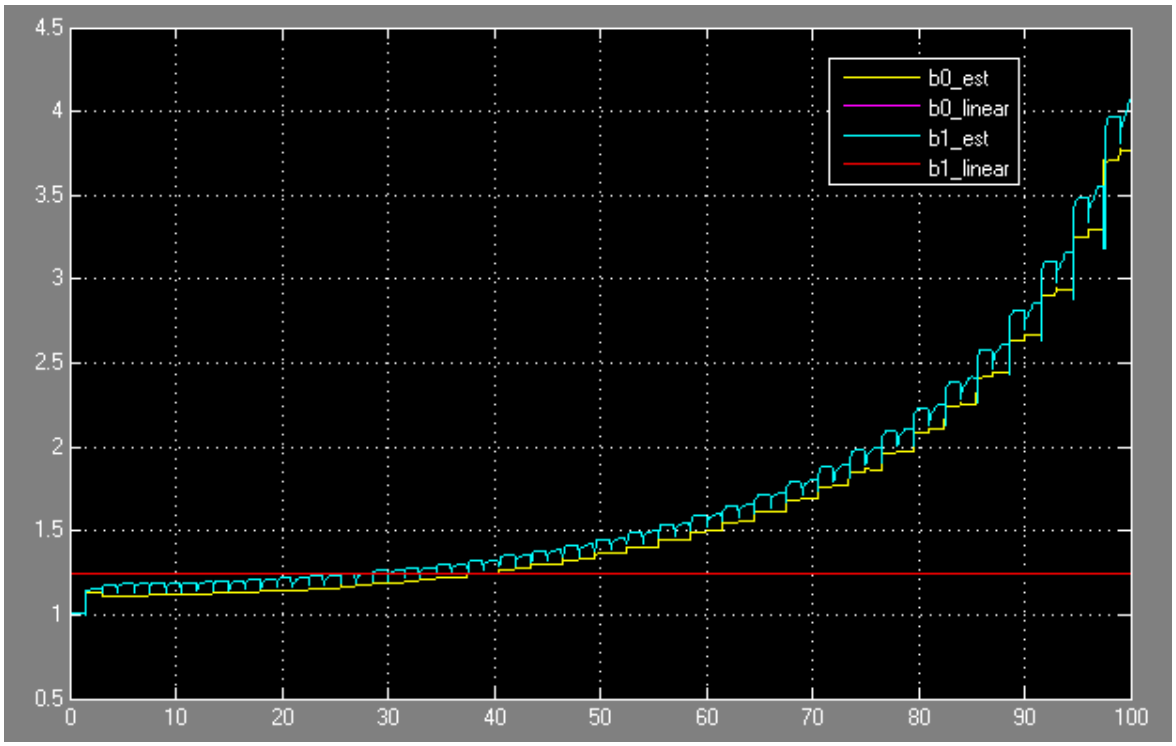


Fig. 22 Estimated B parameter for a [0,10] square signal.

## D. Comparison between output feedback MRAC and ISTR

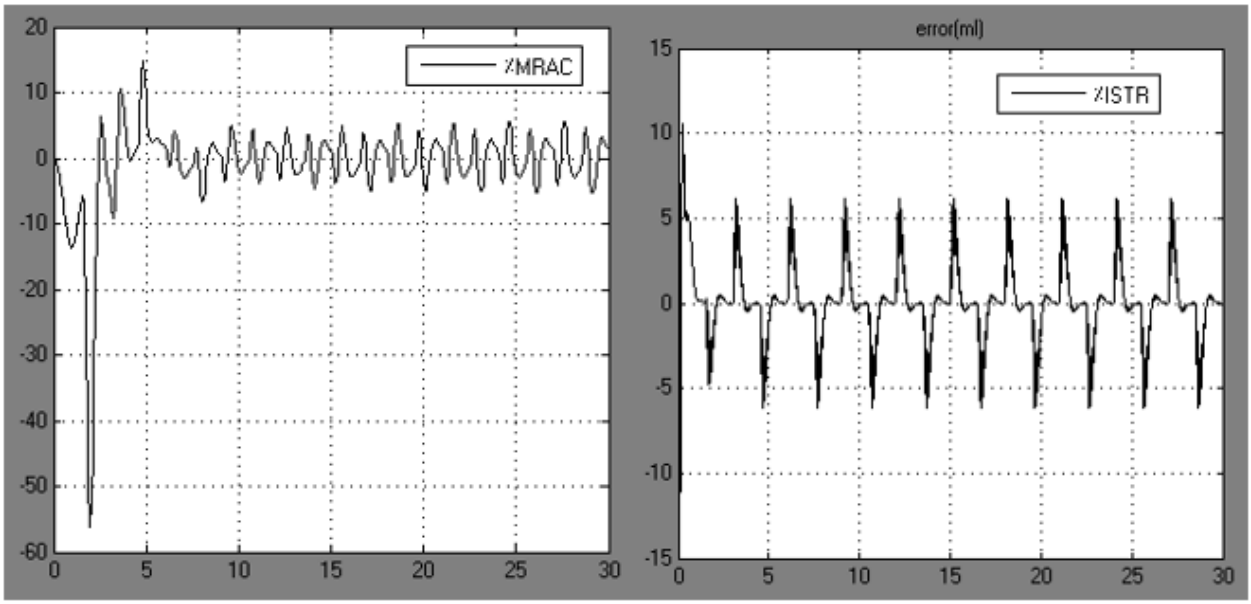


Fig. 23 Percentage error in model matching for the MRAC (left) and the IDST (right) models.

Fig. 23 shows the percentage error in model following for both MRAC and ISTR models. It should noticed that that parameters might not have reached their final values during the simulation period, especially for MRAC, but that gives the general trends. However, It was not found that the error truly goes to zero even with high simulation times. The MRAC model starts with large error that converge fast, but the ISTR has a lower startup error and small ringing that might be due to the sampling period. In conclusion, The ISTR is more desirable at this stage of validation.

## E. Direct Self-Tuning Regulator, Zero Cancelation Case

Fig. 24 and Fig. 25 show a good convergence of the parameters. However, the nonlinear model parameter are not expected to be equal to the linearized model parameters.

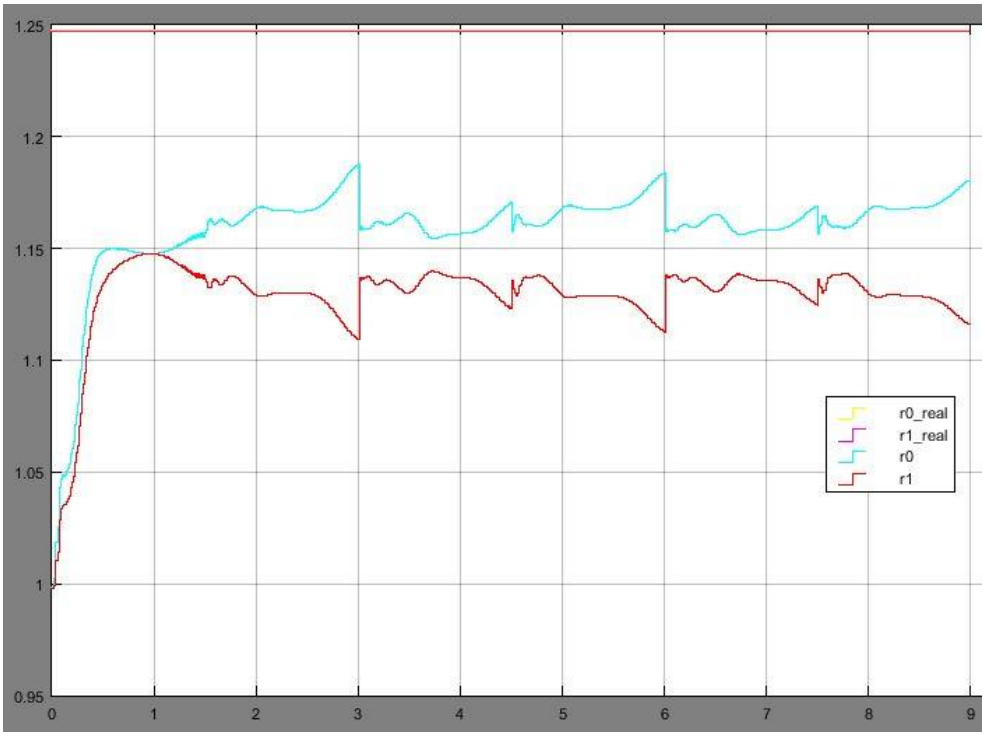


Fig. 24 R Parameters estimation for a square signal with a period of 3 sec.

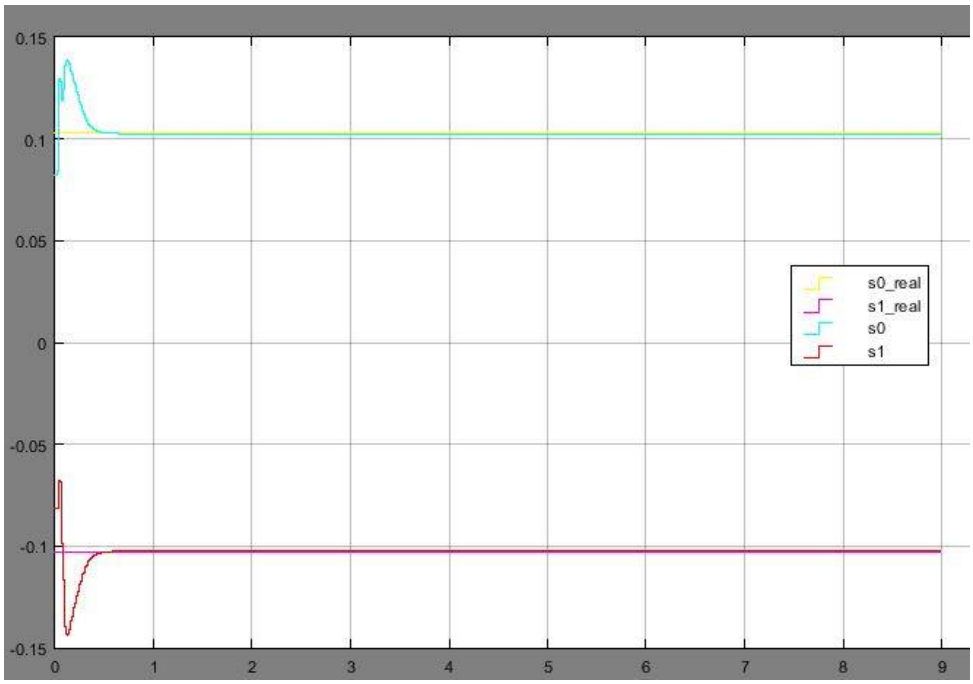


Fig. 25 S Parameters estimation for a square signal with a period of 3 sec.

Fig. 26 shows a good and stable performance of the system for a square input signal. However, it is evident from Fig. 27 that ringing is occurring, which is not desired since that would damage the actuator, and therefore this design is disregarded.

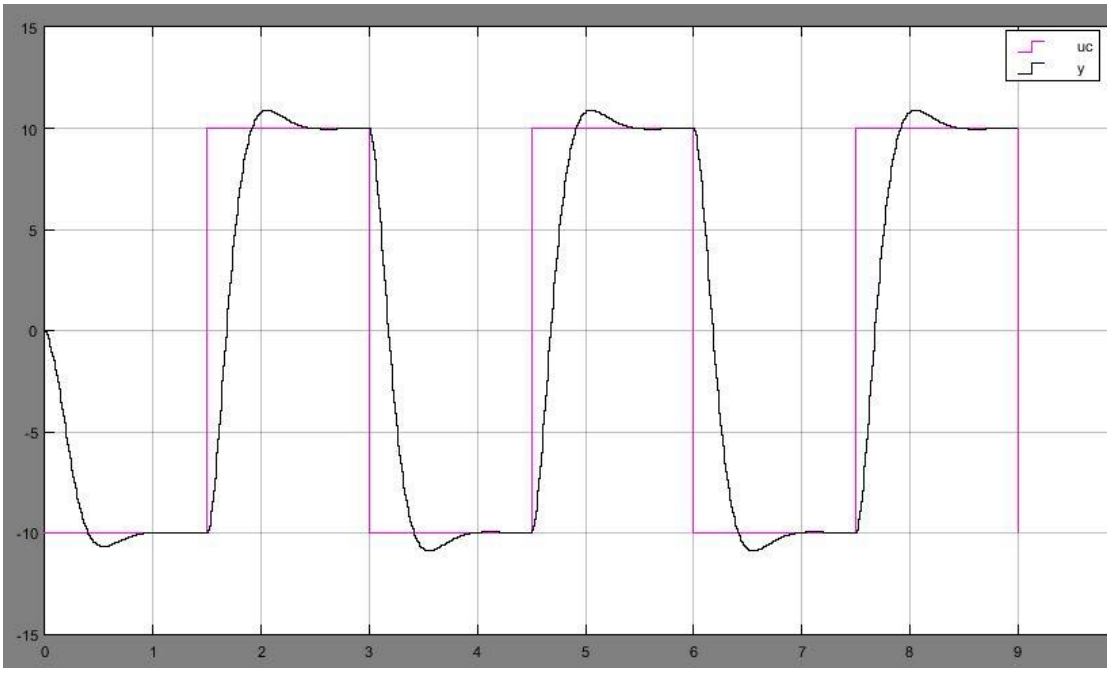


Fig. 26 System response for a square signal [-10,10] of period of 3 sec.

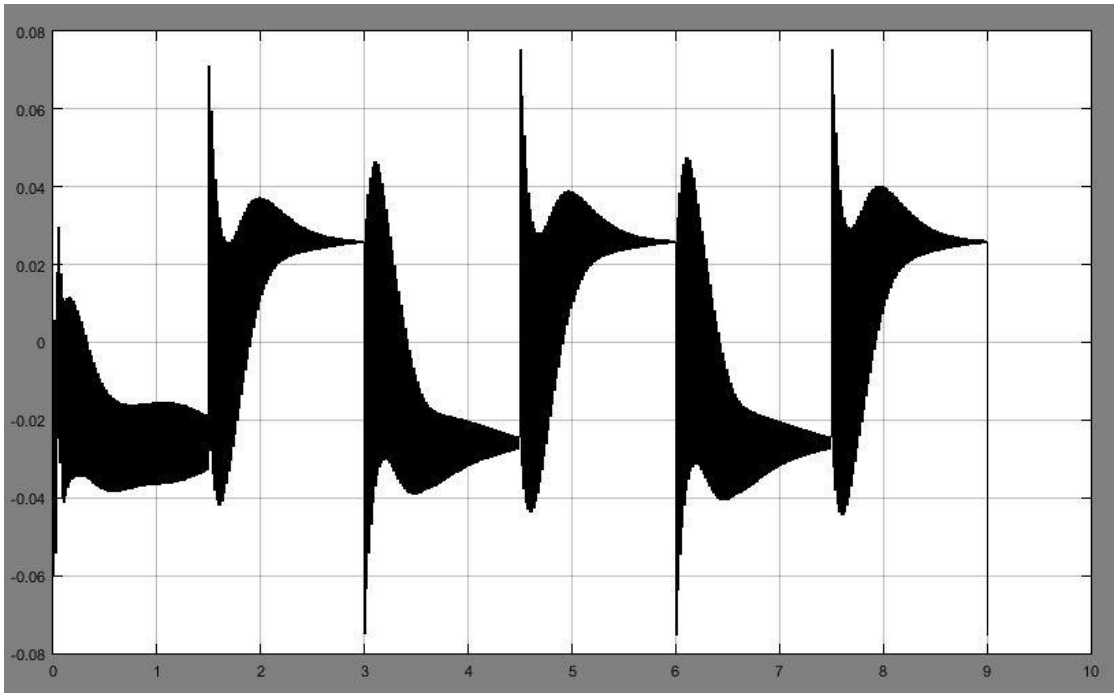


Fig. 27 Input signal for a control square signal [-10,10] of period of 3 sec.

# References

[1] Aghababaei, Amin, and Martin Hexamer. "A new approach to generate arbitrary pulsatile pressure wave forms in mechanical circulatory support systems." *Engineering in Medicine and Biology Society (EMBC), 2015 37th Annual International Conference of the IEEE*. IEEE, 2015.

[2] Arnsparger, John M., et al. "Adaptive control of blood pressure." *Biomedical Engineering, IEEE Transactions on* 3 (1983): 168-176.

[3] Chang, Yu, Bin Gao, and Kaiyun Gu. "A model-free adaptive control to a blood pump based on heart rate." *ASAIO Journal* 57.4 (2011): 262-267.

[4] Hein, Ilmar A., and William Brien. "A flexible blood flow phantom capable of independently producing constant and pulsatile flow with a predictable spatial flow profile for ultrasound flow measurement validations." *Biomedical Engineering, IEEE Transactions on* 39.11 (1992): 1111-1122.

[5] Martin, James F., Alan M. Schneider, and N. Ty Smith. "Multiple-model adaptive control of blood pressure using sodium nitroprusside." *Biomedical Engineering, IEEE Transactions on* 8 (1987): 603-611.

[6] Sahni, Onkar, et al. "Efficient anisotropic adaptive discretization of the cardiovascular system." *Computer Methods in Applied Mechanics and Engineering* 195.41 (2006): 5634-5655.

[7] Yu, Clement, et al. "Multiple-model adaptive predictive control of mean arterial pressure and cardiac output." *Biomedical Engineering, IEEE Transactions on* 39.8 (1992): 765-778.

## APPENDIX A Simulink Representation

### Overall Scheme, Nonlinear Model

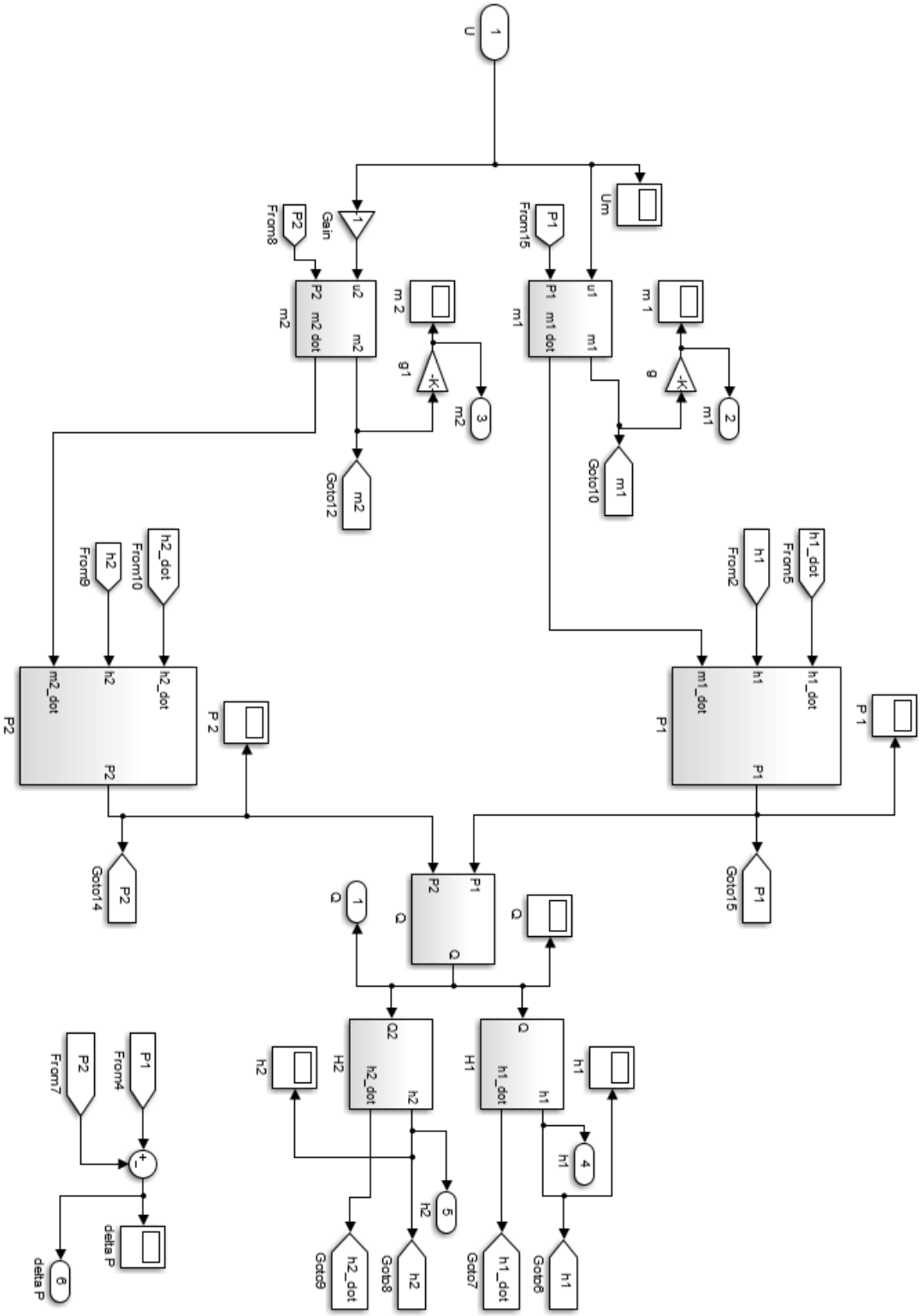

**$m_1$ equation**

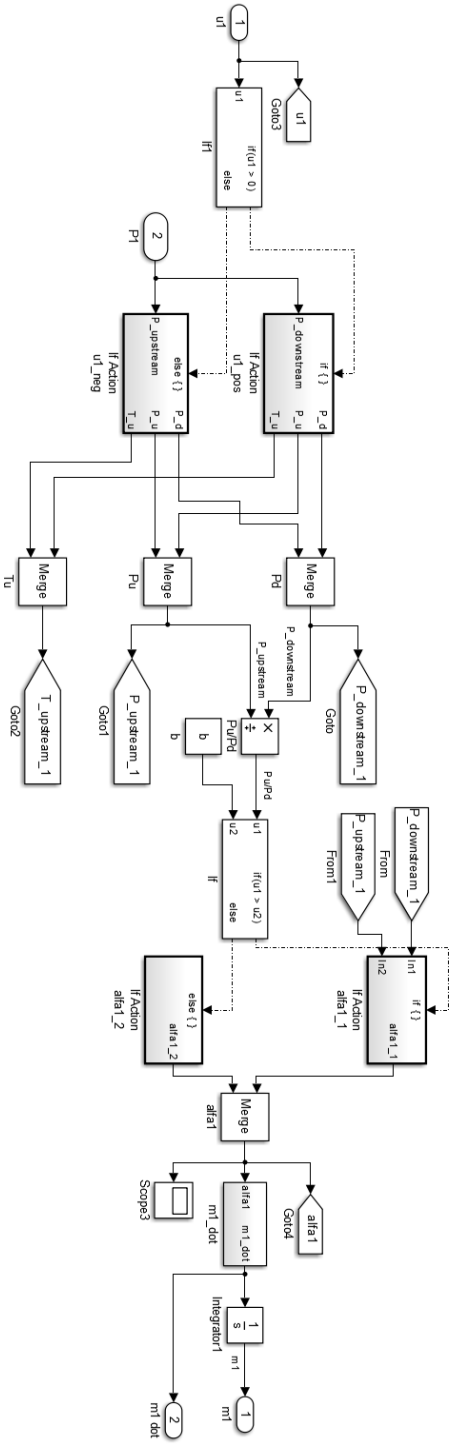
u1
Goto3
If1
P1
P_upstream
If Action u1_neg
P_downstream
If Action u1_pos
Tu
Pu
Pd
Merge
T_upstream_1
Goto2
P_upstream_1
Goto1
b
PuPd
P_downstream_1
Goto
From
From1
If
If Action alfa1_2
If Action alfa1_1
alfa1
Scope3
m1_dot
Goto4
Integrator1
m1
m1 dot

## ISTR Simulink Model

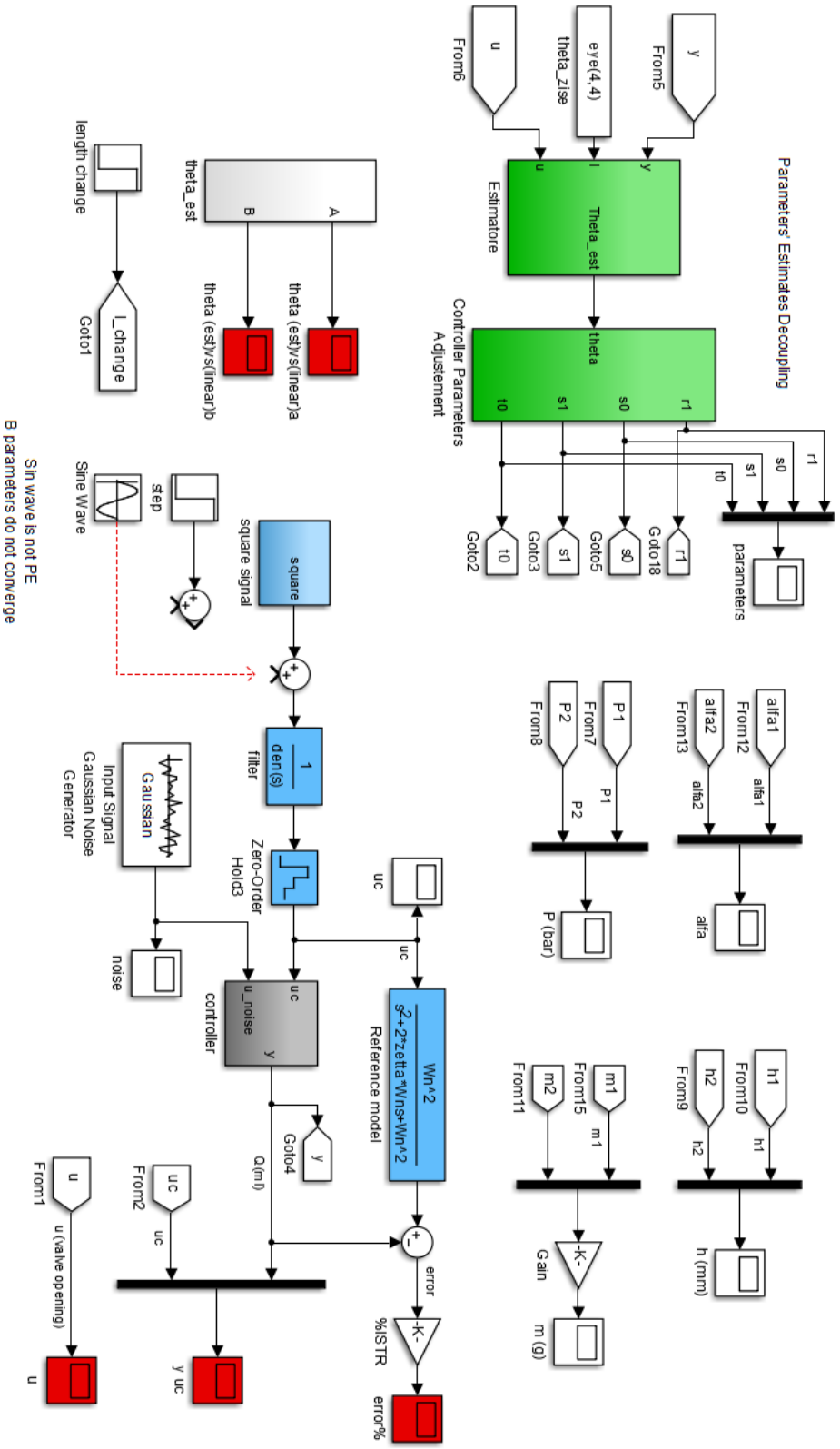

## Controller, ISTR

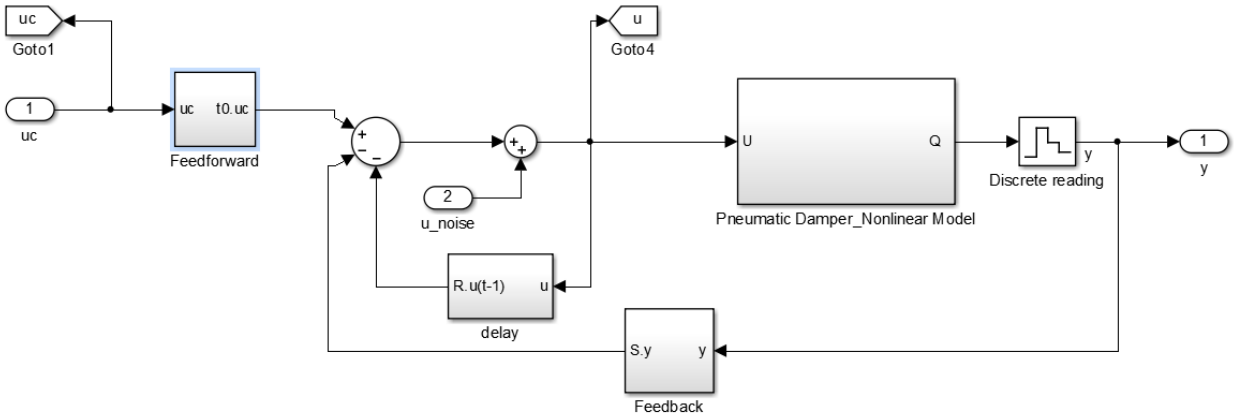

## MRAC output feedback

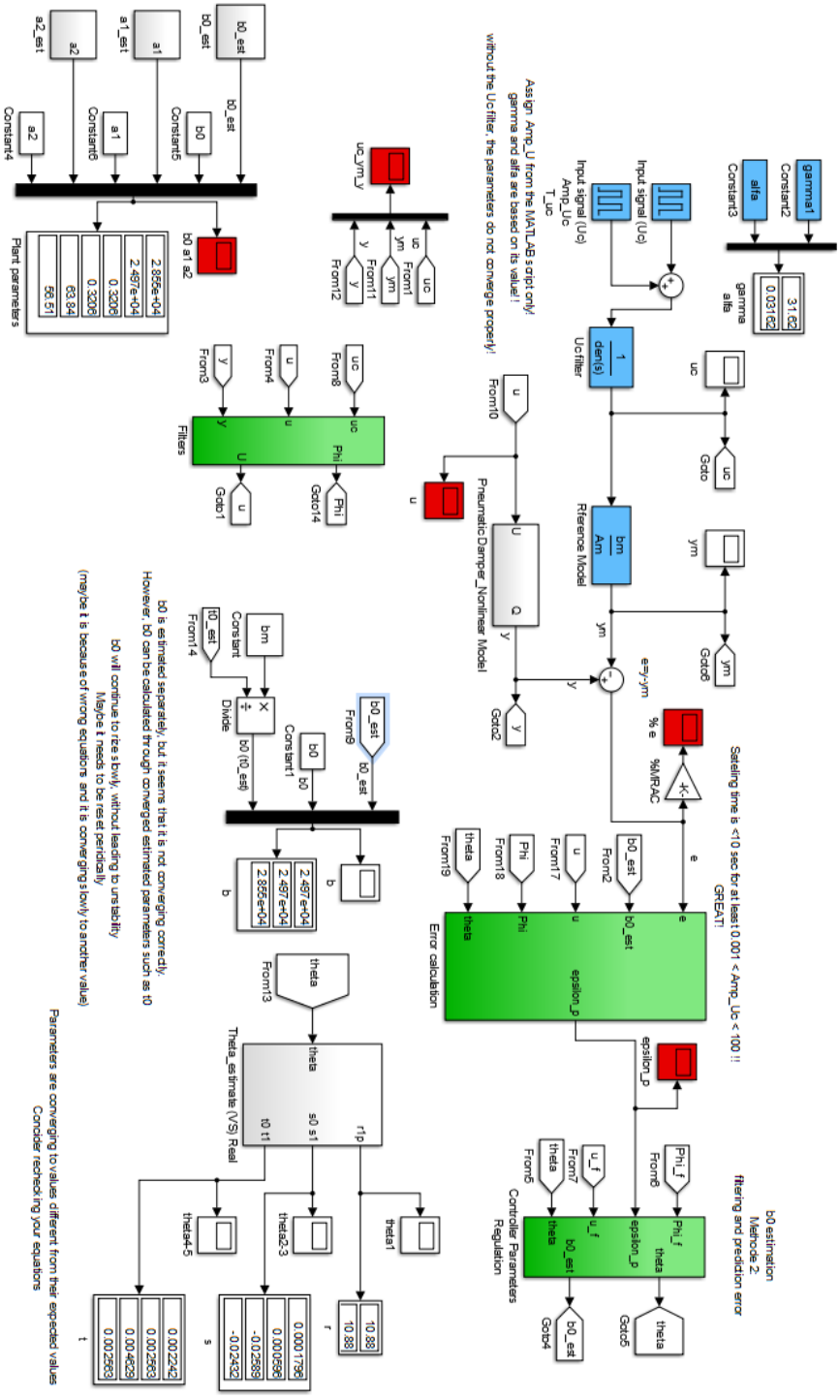

## APPENDIX B Model Parameters

*Air parameters:*

| | |
|---|---|
| $T_1$ | 20℃ |
| $T_2$ | 20℃ |
| $T_0$ | 20℃ |
| $T_S$ | 20℃ |
| $T_f$ | 20℃ |
| $P_S$ | $2\ bar$ |
| $P_0$ | $1\ bar$ |
| $P_{atm}$ | $1\ bar$ |
| $\rho_{air}$ | $1.2 kg/m^3$ |
| $\tilde{R}$ | $287 \times 10^4\ bar\ mm^3/kg\ K$ |
| $\gamma$ | 1.41 |

*Valve coefficients:*

| | |
|---|---|
| $C$ | $0.45 \times 10^{-3}\ m^3/s.bar$ |
| $b$ | 0.21 |

*Pressure chambers parameters:*

| | |
|---|---|
| $D_{ch1}$ | $100\ mm$ |
| $D_{ch2}$ | $100\ mm$ |
| $H_{ch1}$ | $150\ mm$ |
| $H_{ch2}$ | $150\ mm$ |

*Pipe line and water parameters:*

| | |
|---|---|
| $d_{pipe}$ | $10\ mm$ |
| $l_{pipe}$ | $1{,}000\ mm$ |
| $\rho_{water}$ | $998\ kg/m^3$ |
| $\mu$ | $10^{-8}\ bar.s$ |

*Reference model parameters:*

| | |
|---|---|
| $\zeta$ | 0.7 |
| $\omega_n$ | $8\ rad/sec$ |

*Control parameters:*

| | |
|---|---|
| $T_{samp}$ | $0.01\ sec$ |
| $\omega_{n\ filter}$ | $800\ rad/sec$ |

*Adaptive controller (ISTR) parameters:*

| | |
|---|---|
| $\lambda$ | 0.95 |
| $P$ | $eye(4,4)$ |
| $\hat{\theta}_0$ | $0.8\ \theta^0$ |